Fall 2020

Determining variable depth to bedrock using ERT and MASW: A geophysical investigation in St. Louis, MO

Justin James Clinton

Follow this and additional works at: https://scholarsmine.mst.edu/masters_theses

Part of the Geophysics and Seismology Commons

Department:

DETERMINING VARIABLE DEPTH TO BEDROCK USING ERT AND MASW:

A GEOPHYSICAL INVESTIGATION IN ST. LOUIS, MO

by

JUSTIN JAMES CLINTON

A THESIS

Presented to the Faculty of the Graduate School of the

MISSOURI UNIVERSITY OF SCIENCE AND TECHNOLOGY

In Partial Fulfillment of the Requirements for the Degree

MASTER OF SCIENCE

in

GEOLOGICAL ENGINEERING

2020

Approved by:

Dr. David Rodgers, Advisor
Dr. Evgeniy Torgashov
Dr. Kelly Liu

ABSTRACT

The research involves a geophysical study in the Maremec River Valley in St. Louis County, Missouri. The geophysical methods described in this paper can provide a relatively quick, inexpensive, and accurate means in investigating the lithologic characteristics of the subsurface. Method selection is ultimately dependent of the type of investigation and site-specific characteristics. In this investigation, Electrical Resistivity Tomography (ERT) data and Mutli-Channel Analysis of Surface Waves (MASW) data were acquired to image the bedrock beneath the Maremec River to an approximate depth of 110 ft or an elevation of 300 ft for a proposed wastewater tunnel. Two overlapping dipole-dipole arrays were used in a survey across the Maremec River to create a 1,670 ft ERT traverse. The ERT data were then processed to create a 2-D pseudo-section. Multiple MASW surveys were acquired on both sides of the river along the ERT traverse. The MASW data were processed and six shear wave velocity profiles were created. Two borings were logged on both sides of the river near the ERT traverse using material collected from a split-spoon sampler. The data from these geophysical tools were then compared and correlated with the boring data. The depth to bedrock was interpreted to be from 30 ft – 80 ft. The processed MASW data correlated fairly well with the interpreted top-of-rock with 0 ft – 15 ft. Based on the resistivity data, the bedrock can be characterized as fairly weathered beneath ERT stations 600 to 1600. A potential karst feature is present after station 1400 which extends below 300 ft elevation. From ERT stations 100 to 600, the bedrock is considered competent and less weathered.

ACKNOWLEDGEMENTS

TABLE OF CONTENTS

LIST OF ILLUSTRATIONS

Page

LIST OF TABLES

1. INTRODUCTION

In Missouri, bedrock is mainly comprised of Pennsylvanian, Mississippian, Ordovician, and Cambrian age strata. Bedrock depth typically can vary across the state from 0 to over 200 ft. Over the last 20 years, geophysical investigations using the Electrical Resistivity Tomography (ERT) and Multi-Channel Analysis of Surface Waves (MASW) tools have become more commonly used to investigate the subsurface and bedrock. This is due to the fact that geophysical methods such as the ERT and MASW can be very effective when enhanced by ground truth. These data can be acquired at a relatively low cost when compared to other subsurface investigative techniques. These geophysical techniques can be used to image bedrock for a variety of different subsurface investigations including imaging karst features, fracture zones, locating tunnels, groundwater flow, and mineral exploration.

In this paper, a case study is discussed, description of the regional geology is given, and the concepts behind each method used are explained in detail. The ERT and MASW methods were used primarily to image the bedrock to a depth of at least 110 ft or an elevation of 300 ft; determine the elevation of the top of bedrock; determine the soil thickness in the Maremec River Valley; and characterize the subsurface soil and rock quality. The ERT data were acquired to an approximate depth of 150 ft. and the MASW data were acquired to an approximate depth of 100 ft. The ERT and MASW data were compared and constrained with multiple borehole data.

2. PURPOSE AND SCOPE OF STUDY

The primary goal of the geophysical study was to determine if a site in the Meramec River Valley in southeast St. Louis County was a suitable location for a proposed wastewater tunnel. This was accomplished by collecting, processing, and interpreting Electrical Resistivity Tomography (ERT) data and Multichannel Analysis of Surface Waves (MASW) data with the aid of boreholes. These data were used to effectively determine the variable depth to bedrock and characterize the soil and bedrock lithology as well as identify any anomalous zones. The interpreted depth to the top-of-rock generated by ERT and MASW methods will be compared with borehole data from multiple sources.

3. REGIONAL GEOLOGY

According to the Missouri Department of Natural Resources (MDNR), Missouri's landscape consists of five geologic provinces: Dissected Till Plains, Osage Plains, Salem Plateau, Springfield Plateau, and Mississippi Alluvial Plains as shown in Figure 3.1 this section briefly describes the regional geology of St. Louis County. It is beyond the scope of this section to discuss all the geologic provinces, structural, and stratigraphic settings in Missouri in much detail.

The bedrock of the Dissected Till Plains province is primarily Pennsylvanian age except along the eastern edge of Missouri which is Mississippian age (Figure 3.2). This portion extends through almost half of the St. Louis area and covers most of St. Louis County. The southernmost extent of the Pleistocene glaciation extends across Missouri along the Missouri River and through the northern half of St. Louis County.

The majority of the river valleys in this region are comprised of Holocene age alluvium consisting of gravel, sand, and silt. The valley soil and can range from 0 to 215 feet thick (Harrison, 1997). The surficial material of the St. Louis County, (MDNR Surficial Materials of Missouri, 2002) is comprised of residuum consisting of clays and gravels from cherty limestone and can range from 0 to 50 feet thick.

The Salem Plateau is mainly covered by residuum from cherty dolomite and sandstone comprised of clay, silt, sand, gravel, and boulders. The thickness of the residuum in this province can vary from less than 10 ft up to 200 ft in some areas. Mississippian-age limestone of the Salem, Warsaw, and Keokuk-Burlington formations form the bedrock surface in the St. Louis County area which overlie the Ordovician and Cambrian strata

(Figure 3.3). Even though these same Mississippian age formations are found in the Springfield Plateau, it is still considered part of the Salem Plateau by MDNR. Silurian and Devonian age strata are not present.

In east-central Missouri, the Warsaw formation is the lowest member of the Meramecian series and conformably overlies the Burlington-Keokuk formations (Figure 3.4). The Warsaw composition varies from coarse crystalline limestone to dolomitic and very shaly, limestone and a thickness range from 80 to 100 feet. The underlying Burlington-Keokuk, Fern Glenn, and Chouteau group formations form the Osagean series. The Burlington-Keokuk limestone are comprised of light grey-bluish grey, coarse crystalline limestone with abundant chert beds. The thickness of these formations ranges from 70 to 100 feet and 50 to 100 feet and is considered fairly uniform. Although the Burlington and Keokuk are separate formations, they are often lumped together because the boundary between the two can be very difficult to identify (Howe, 1961).

Ordovician and Cambrian rocks are primarily dolomite and sandstone. The Ordovician bedrock (Figure 3.3) that makes up much of the Salem Plateau consists of the Maquoketa Group, the Cape and Kimmswick limestone, the Decorah and Plattin Groups, Joachim dolomite, St. Peter sandstone, Smithville dolomite, Powell dolomite, Cotter dolomite, Jefferson City dolomite, Roubidoux Formation, and the Gasconade dolomite.
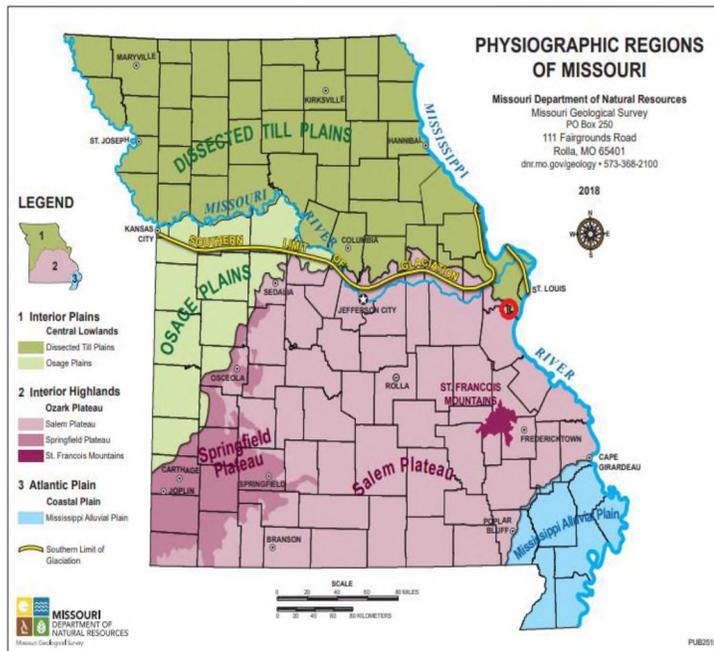
Figure 3.1. Geologic provinces of Missouri. Site location (red circle) and geologic provinces of Missouri (MDNR, 2018).
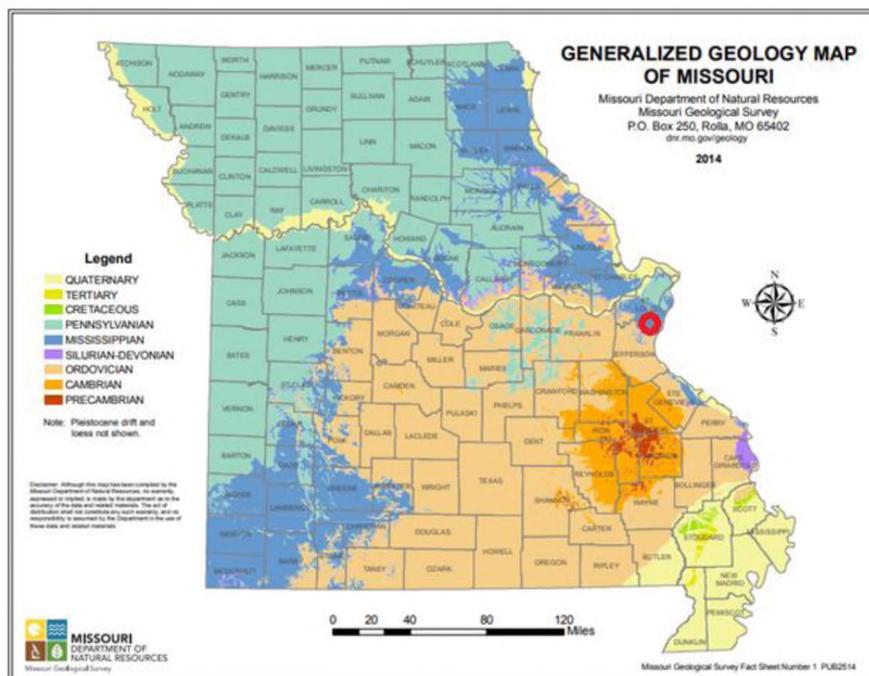
Figure 3.2. Generalized geologic map of Missouri. Site location and bedrock geology of Missouri (MDNR, 2014).
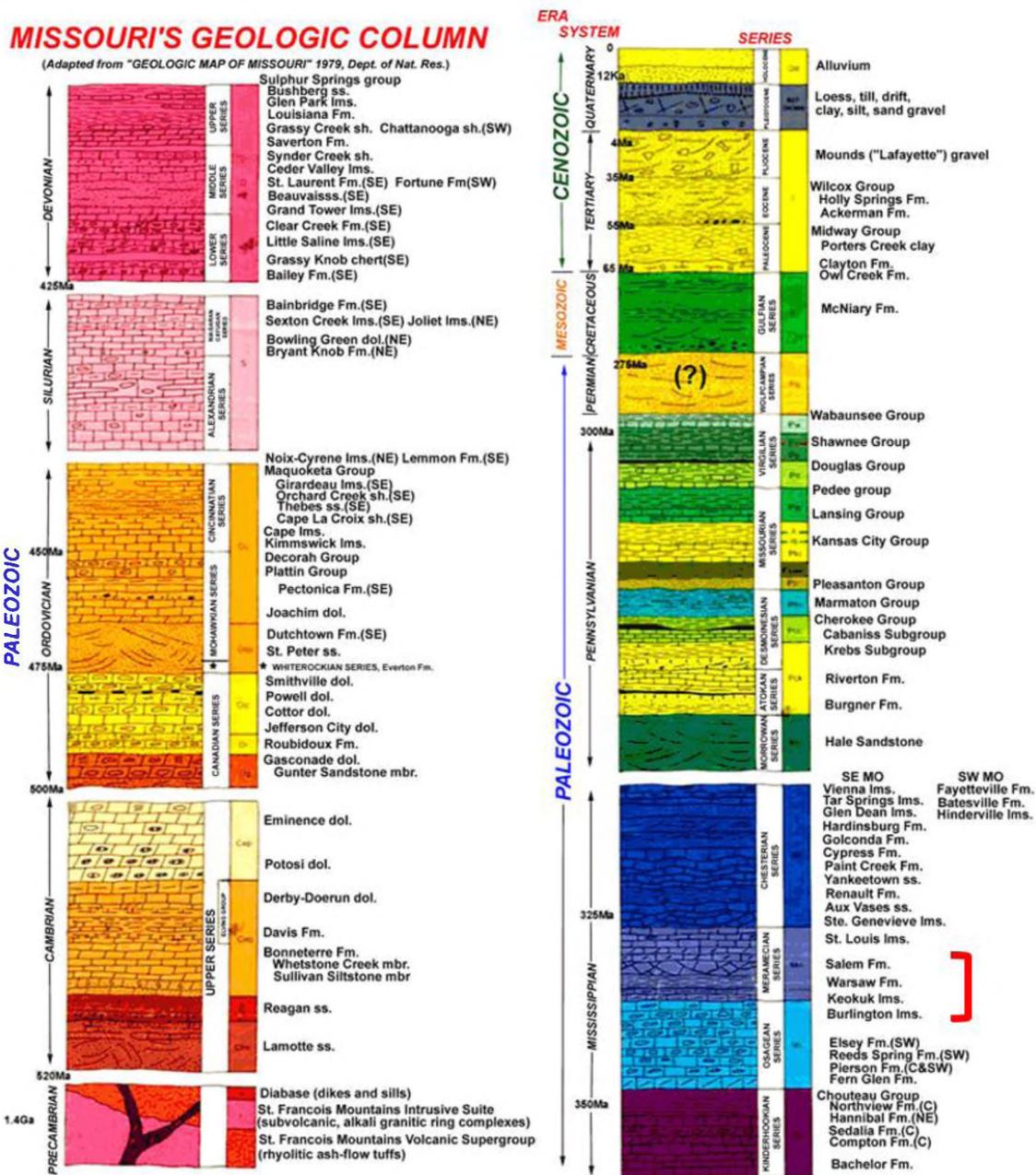
Figure 3.3. The stratigraphic column of Missouri. The red line marks the formations that form the bedrock in the study area (mofossils.com).
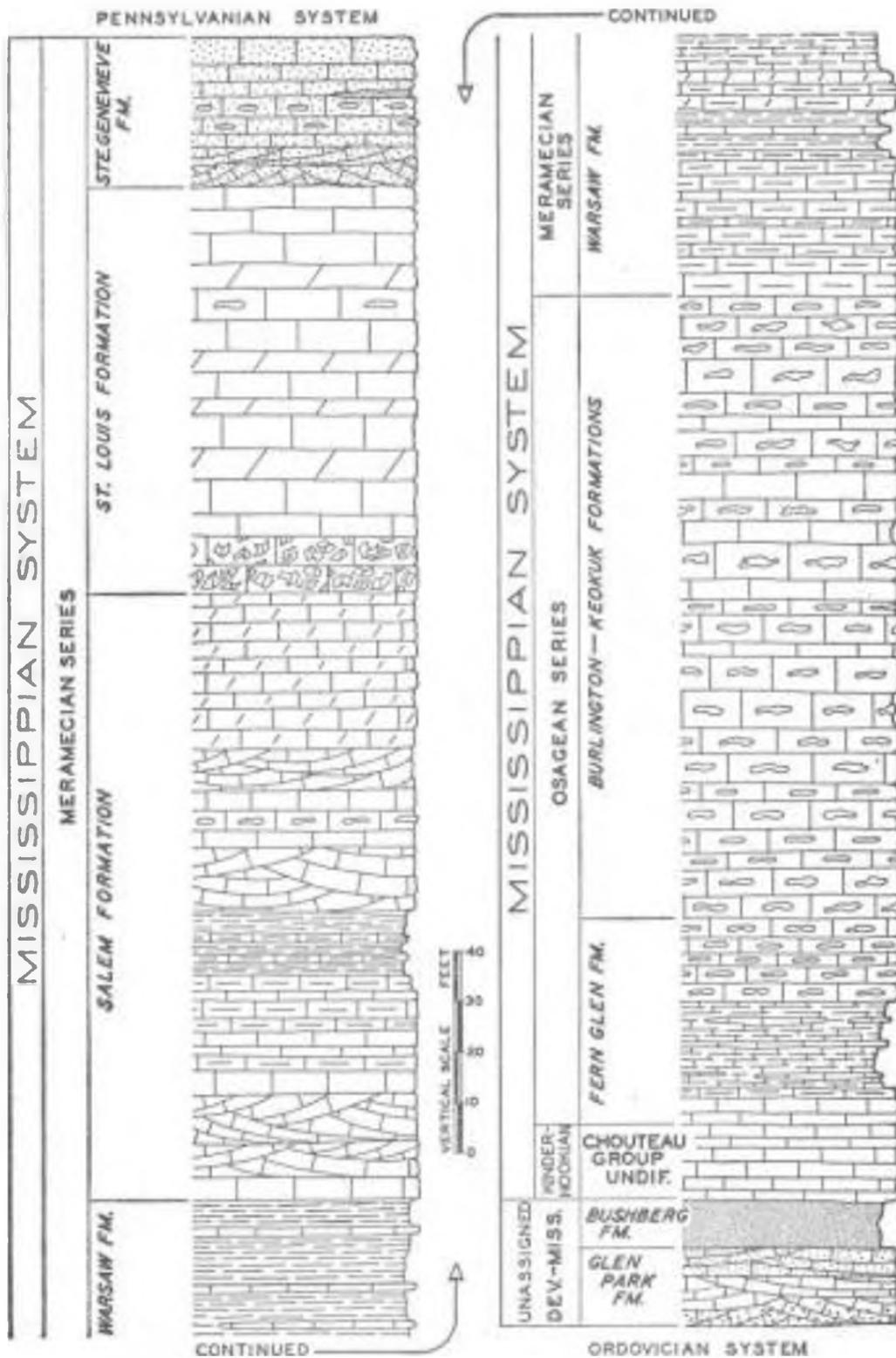
Figure 3.4. Stratigraphic column of the Mississippian System. Mississippian System stratigraphic column for east central Missouri (Howe, 1961).

4. OTHER INVESTIGATION METHODS

Common methods for investigating soil and bedrock include borings such as coring, augering, and excavation. Coring involves a hollow drill bit that is designed to cut through soil and rock and collect a sample inside the drill stem. Augers can be used in unconsolidated material to collect similar data. Augers feed material up to the surface of the borehole where samples and observations can be noted. Augers can be solid or hollow stem sampling. Hollow stem augers collect a disturbed boring sample inside the stem while bringing auger cuttings to the surface. Solid stem augers do not recover boring samples, but the cuttings are recorded. Excavation usually involves creating test pits and trenches to observe the subsurface. These methods can provide great information about the soil and bedrock characteristics in a specific location. These methods are necessary today for drilling wells and characterizing the subsurface for potential building sites. However, these methods are very expensive, labor intensive, and time consuming as well as destructive. Difficult terrain can also create issues. Because of this, borings cannot be done everywhere. Instead, geophysical techniques can be used to correlate data between boreholes. The borehole data is often used as an important aid to enhance geophysical data and to help confirm interpretations.

Geophysical techniques for investigation bedrock can include gravimetry, electromagnetics, ground penetrating radar (GPR), seismic refraction/reflection, electrical resistivity, and multi-channel analysis of surface waves (MASW). Gravimetry can be very difficult to acquire and process without have extensive knowledge of the parameters and can be very erroneous. Electromagnetics (TDEM/FDEM) can be very useful for mapping

bedrock and soil depth but are site dependent and cannot measure the strength of the soil/rock materials (Anderson, 2017). GPR is commonly used for imaging the subsurface for a variety of investigations. However, the main pitfall with using GPR is that it cannot penetrate through soil containing abundant clay minerals. Clay is abundant in the surficial materials of Missouri. Since the electrical resistivity and MASW methods can perform very well in clay rich environments with good lateral and vertical resolution and given the survey location, these methods were chosen for the study.

5. RESEARCH METHODOLOGY

The following is a detailed explanation and illustration of the methods used in this study. Research was conducted using Electrical Resistivity Tomography (ERT) and Multi-Channel Analysis of Surface Waves (MASW). Explanations include the concept or theory behind these geophysical tools; the data acquisition and processing; and the interpretation of data. Echo Sounding and Side Scan Sonar data were collected across the marine portion of the study area to assist with the processing and interpretation of the ERT data and not discussed in detail.

5.1.   ELECTRICAL RESISTIVITY TOMOGRAPHY (ERT)

Electrical Resistivity Tomography (ERT) can be used in many different applications which include mapping variable depth to bedrock, locating voids (caves, tunnels, abandoned mines, etc.), mapping sand and gravel lenses, and mapping contaminants. Resistivity surveying techniques include vertical electric sounding, profiling, and a combination of profiling and sounding (tomography). These techniques are performed by using a pre-determined array of electrodes. There are several standard array types that have been developed. The basic function of all these techniques is to measure the spatial variations in potential differences as a result of an induced current. These potential differences are used to determine the resistivity. The resistivity distributions across the survey can then be displayed to create an image or pseudo-section (Figure 5.1). The resistivity image can be interpreted to create a geologic model. These data when supplemented with external constraints such as borings or ground truth, help refine and

characterize the subsurface, both soil and bedrock. This is possible because soil and rock materials exhibit different resistivity variations caused by the differences in mineral content, water content and saturation, porosity, and permeability (Loke, 1999).
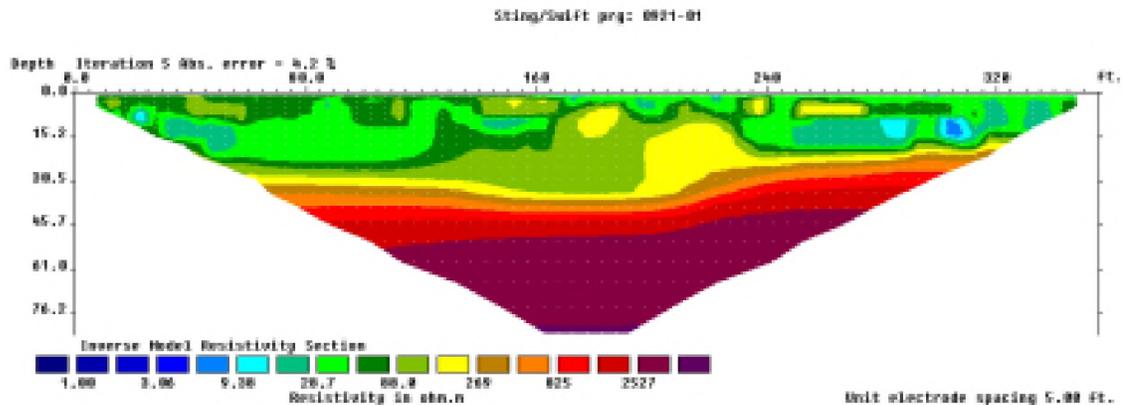
Figure 5.1. Example pseudo-section. Example of a typical 2-D pseudo-section of the area. Nwokebuihe, S. C. (2014).

5.1.1. Geology and Resistivity. According to Loke (1996-2016) and Robinson and Coruh (1988) the conduction of current through the ground can come in three different forms. Two of which primarily occur as either electronic or Ohmic conduction, or electrolytic conduction. The third is dielectric conduction. Electronic conduction is the current flow through materials such as native metals. The current travels using free electrons which move through the metals crystalline structure. Electrolytic conduction is one that occurs from the presence of dissolved ions in the pore water or groundwater. This type is the most common. Dielectric conduction involves cyclical shifting of ions in a crystalline structure that is an insulator. This type is looked at as alternating current. No current flow actually takes place.

5.1.2. Concept of Electrical Resistivity. A simple definition of resistance (R) is the opposition to the flow of current through a material. Resistance is measured in ohms. One ohm is equal to the resistance between two points when a constant electromotive force (EMF; measured in voltage (V)) applied between two points produces a current of one ampere (amp (I)). The induced current (measured in amps) is driven by an EMF that creates a potential difference caused by the resistance (R) between the two terminals or electrodes (Van Valkenburgh, Nooger, and Neville, 1992). Because of the potential differences between the electrodes, the current is compelled to flow along paths from the source to the sink (Robinson and Coruh, 1988). The voltage is the measure of the potential differences created from the current flow between the electrodes. This concept of resistance (R) can be applied to the earth subsurface. The earth is the resistor component of the circuit. Ohm's Law controls the flow of electrical currents through the subsurface and it is limited to current flow below a saturation level (Robinson and Coruh, 1988). This basic law of physics is used in all electrical resistivity surveying (Loke, 1996-2016). Ohm's law can be represented by the following equation:

$$V = IR \tag{1}$$

where V = Voltage, I = Induced Current, and R = Resistance.

To understand the application of electrical resistivity in geology, consider Figure 5.2. The resistance (Ω) in a cylinder of any material, such as soil or rock, can be expressed as the resistance between the opposite faces of the cylinder (Keary and Brooks, 1991). Using a cylinder of soil/rock material as the resistor in the circuit and applying a known voltage and current across the cylinder
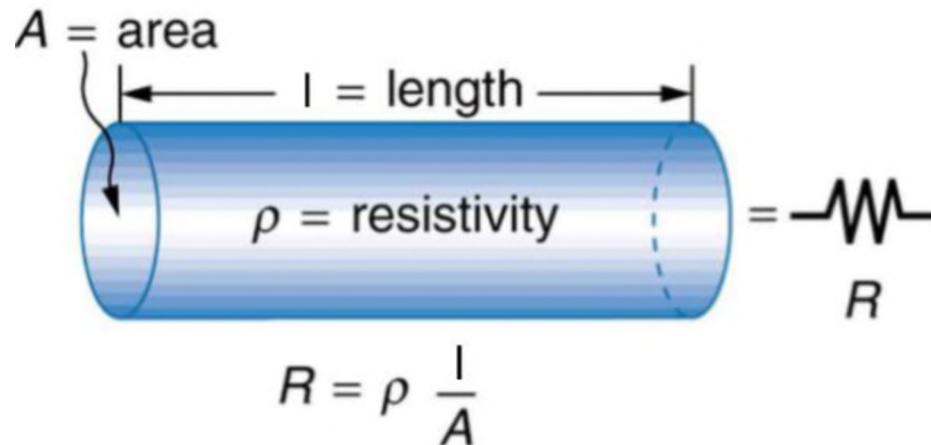
Figure 5.2. Cylinder circuit and Ohm's Law (*Khanacademy.org*, 2020).

Ohm's Law can be rewritten from equation 1 as:

$$R = \rho * L/A \qquad (2)$$

where R, is the resistance;

ρ represents the resistivity of a homogeneous soil/rock material;

L is the length of the cylinder;

and A is the cross-sectional area of the cylinder.

These parameters control the overall resistance (R). R is inversely proportional to the cross-sectional area (A), so increasing/decreasing A will decrease/increase R. Transposing parameters, equation 2 can be rewritten as:

$$\rho = R * A/L \qquad (3)$$

The concentration of current passing through the cross-sectional area of the resistor is known as the current density (μ) and can be defined by the following equation (Robinson and Coruh, 1988):

$$\mu = I/A \qquad (4)$$

The resistivity (ρ) is inversely proportional to the length of the cylinder (L). The resistivity of a material (ρ) is an intrinsic characteristic which defines how readily a material will transmit a current. Therefore, ρ is dependent on the molecular composition and dimensions of the materials (*Khanacademy.org*, 2020). In a homogenous material, ρ is constant regardless of where the source and sink electrodes are placed. However, in reality, the subsurface is heterogeneous and the materials present beneath the surface are often not known for certain. Because of this, apparent resistivity (ρ_a) is used to represent a weighted average of the resistivity in the heterogeneous subsurface (Robinson and Coruh, 1988). The apparent resistivity can be determined from the following equation:

$$\rho_a = kV/I \hspace{4cm} (5)$$

where k represents the geometric factor for the desired array configuration and it is different for each array and determined by both electrode spacing and surface location. The geometric factor will be discussed in more detail.

5.1.3. Theory of Resistivity and the Subsurface. Much of the concepts and theories discussed in this section are material covered in Basic Exploration Geophysics by Edwin S. Robinson and Cahit Coruh, 1988. To explain this theory, two electrodes are current electrodes that represent the source (source electrodes) and the other two are voltmeter electrodes (sink electrodes) that represent the current sink (Figure 5.3). Current flow travels along paths through the ground in all directions via the source electrode. To determine the directions of the paths, the effects of both the source and sink are considered (Robinson and Coruh, 1988). It is assumed that the ground has a constant resistivity. Because the current is confined to the subsurface, this creates a hemispherical half-space

made up of current flow lines and equipotential surfaces (Figure 5.4). This hemisphere can be called a resistor.

To determine any potential difference, it is assumed that the earth subsurface and the hemisphere half space are uniform and homogenous. The resistivity is uniform and current flows in all directions away from the source uniformly (Figure 5.4). The current flow lines as shown in Figure 5.4 (b) and (c), converge on the sink electrode. When source and sink are sufficiently separated, current flow lines near the source travel outward equally in all directions. Near the sink, current flow lines converge equally from all directions if the resistivity of the media is uniform. Perpendicular to the current flow lines are equipotential surfaces on which the potential is constant everywhere (Robinson and Coruh, 1988). Assume the resistance encountered by the current flow has traveled a distance (D) from the source. Current flow radiates out in all directions and through the hemispherical half space. When the current leaves this space, it travels across the area of $2\pi D^2$ which represents the surface of the hemisphere. From equation 2, R can be expressed by the product of ρ and D that the current travels divided by the area $2\pi D^2$ across which it must flow (Robinson and Coruh, 1988):

$$R = \frac{\rho D}{2\pi D^2} \tag{6}$$

which equates to:

$$R = \frac{\rho}{2\pi}\left(\frac{1}{D}\right) \tag{7}$$

The resulting change in potential from the current flow through the hemisphere can be determined from equation 1:

$$V = IR = \frac{\rho I}{2\pi}\left(\frac{1}{D}\right) = V_0 - V_D \tag{8}$$

Equation 8 is the difference between the electric potential V_0 at the source and the electric potential V_D at any point in the subsurface at distance D from the source electrode. The hemisphere surface of radius D contains all points at this distance. This means that the electric potential related to current flow from the source is the same anywhere on that surface (Robinson and Coruh, 1988). Such a surface is called an equipotential surface. The potential for the sink is denoted as $-V_0$ since current flows converge on the sink. The current that travels to the sink encounters resistance that can be in analyzed in terms of that hemispherical space that it flows through. All the points at a distance D from the sink, in which the current flows from, are compelled to travel through the hemispherical space that is the same as the space around the source with an equal radius. The resistance of the hemispherical space at the sink can be defined as:

$$-V = IR = \frac{\rho I}{2\pi}\left(\frac{1}{D}\right) = V_D - V_0 \qquad (9)$$

This equation can be used to determine the potential difference sink potential (- V_0) and the potential for all points at distance D (V_D) (Robinson and Coruh, 1988). V can be found at any point in the subsurface by adding both inputs from source and sink together to form the following equation:

$$V = \frac{\rho I}{2\pi}\left(\frac{1}{D_1} - \frac{1}{D_2}\right) \qquad (10)$$

D_1 is the distance to the source electrode

D_2 is the distance to the sink electrode

This can be further explained with Figure 5.3. In Figure 5.3 (b), an array with electrodes A(source), M and N (voltmeter), B(sink) is shown. M can be at a distance D_1 from the source and D_2 from the sink and N can be at a distance D_3 from the source and D_4

from the sink. The potential measured at M and N can be determined by substituting D_1 and D_2 and D_3 and D_4 in equation 10 to find V_M and V_N (Robinson and Coruh, 1988). This is the determination of apparent resistivity. The potential difference measured by M and N is expressed:

$$V_{MN} = V_M - V_N = \frac{\rho I}{2\pi}\left(\frac{1}{D_1} - \frac{1}{D_2} - \frac{1}{D_3} + \frac{1}{D_4}\right) \tag{11}$$

Rearrange for ρ:

$$\rho = 2\pi \frac{V_{MN}}{I}\left(\frac{1}{D_1} - \frac{1}{D_2} - \frac{1}{D_3} + \frac{1}{D_4}\right)^{-1} = \frac{V_{MN}}{I}k = \rho_a \tag{12}$$

where k is the geometric factor and is expressed as:

$$k = \frac{2\pi}{\frac{1}{D_1} - \frac{1}{D_2} - \frac{1}{D_3} + \frac{1}{D_4}} \tag{13}$$

Equation 10 can be used to determine points of equal potential that make up the equipotential surface. Current flow lines are always perpendicular when they intersect the equipotential surface as shown in Figure 5.3 and Figure 5.5. To understand how resistivity can be determined across different media, it is important to how current density changes across different media boundaries. The current density describes how the charges that make the current are spaced apart as it moves through a medium (Robinson and Coruh, 1988). Consider equation 2 and equation 4. Equation 4 can be transposed to:

$$I = \mu A$$

Equation 2 and 4 can be substituted into equation 1 to represent current density where:

$$V = \frac{\rho L}{A}(\mu A) = \mu\rho L$$

This can be expressed in terms of μ:

$$\mu = \frac{V}{\rho L} \tag{14}$$

In Figure 5.5, current flow lines intersect the equipotential surfaces at a number of points a-g. Between each surface, there are segments of current that denote intervals of equal change in V. The length of these segments is proportional to the spacing of charges that comprise the current. The lengths of these intervals increase as depth increases or as the distance from the source and sink electrode increases (Robinson and Coruh, 1988). The soil/rock material density can be expressed by equation 14 where L is the length of the interval between each point. The density can be determined for each interval. As μ increases, the spacing between the charges that makes up the current decreases. As μ decreases, this spacing increases. μ decreases as the distance increases from the source and sink electrodes. This is because the lengths of each path segment increase while there are no corresponding changes in potential The current density and potentials are different across the equipotential surfaces (Keary and Brooks, 1991).

Figure 5.6 illustrates that where there are different media interfaces with contrasting resistivity, such as stratagraphic boundaries, current flow is preferentially channeled into the less resistive media. The current density is highest in the media with lowest resistivity. In situations where strata have horizontal interfaces, the current flow is symmetrical. In situations where there is a vertical interface for instance, a boundary between tilted stratigraphy, fault, or dike, current flow density will be highest in the lowest resistivity media and current flow will be asymmetrical.
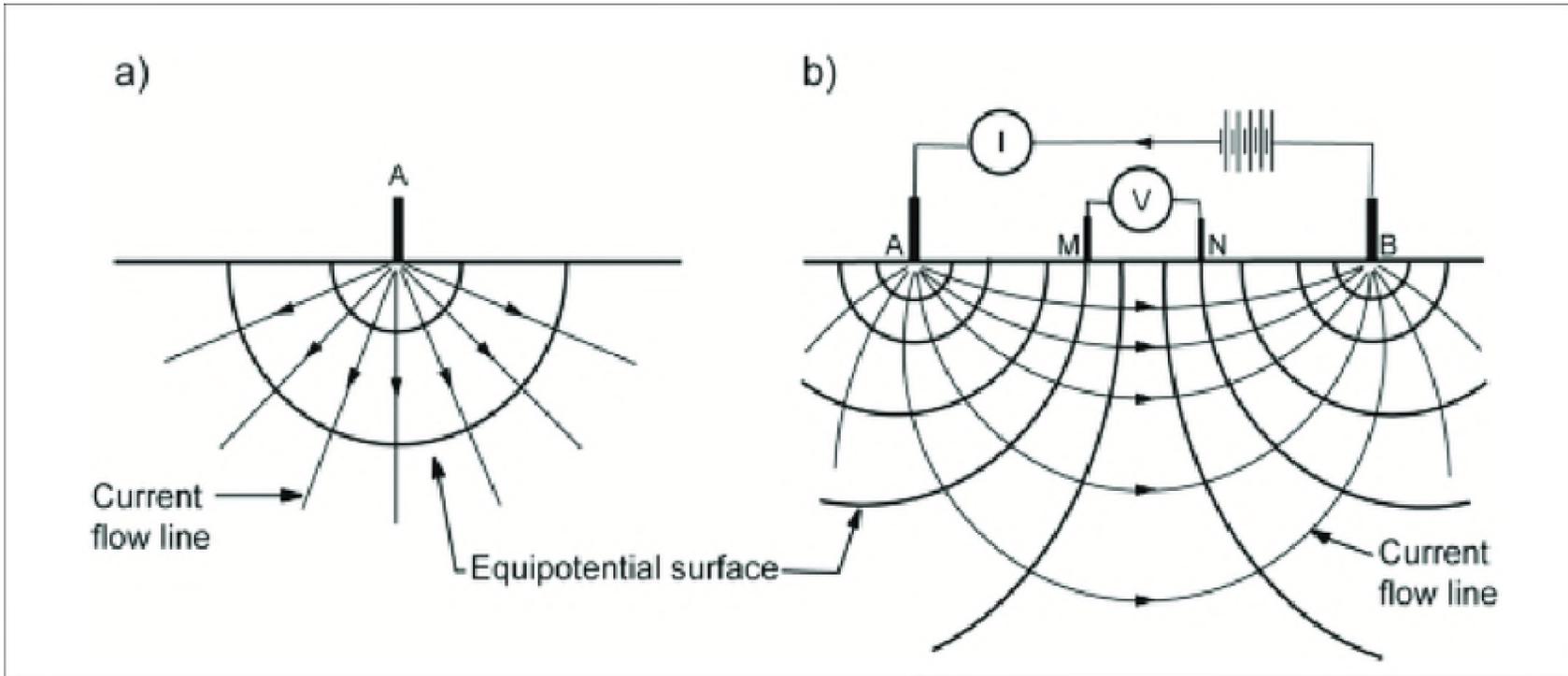
Figure 5.3. Current flow lines and equipotential surfaces. Figure (a) Current or source electrode and figure (b) a simple four electrode array with current source (A and B) and current sink (M and N). These figures illustrate current flow lines and equipotential surfaces with a general array in a homogeneous subsurface.
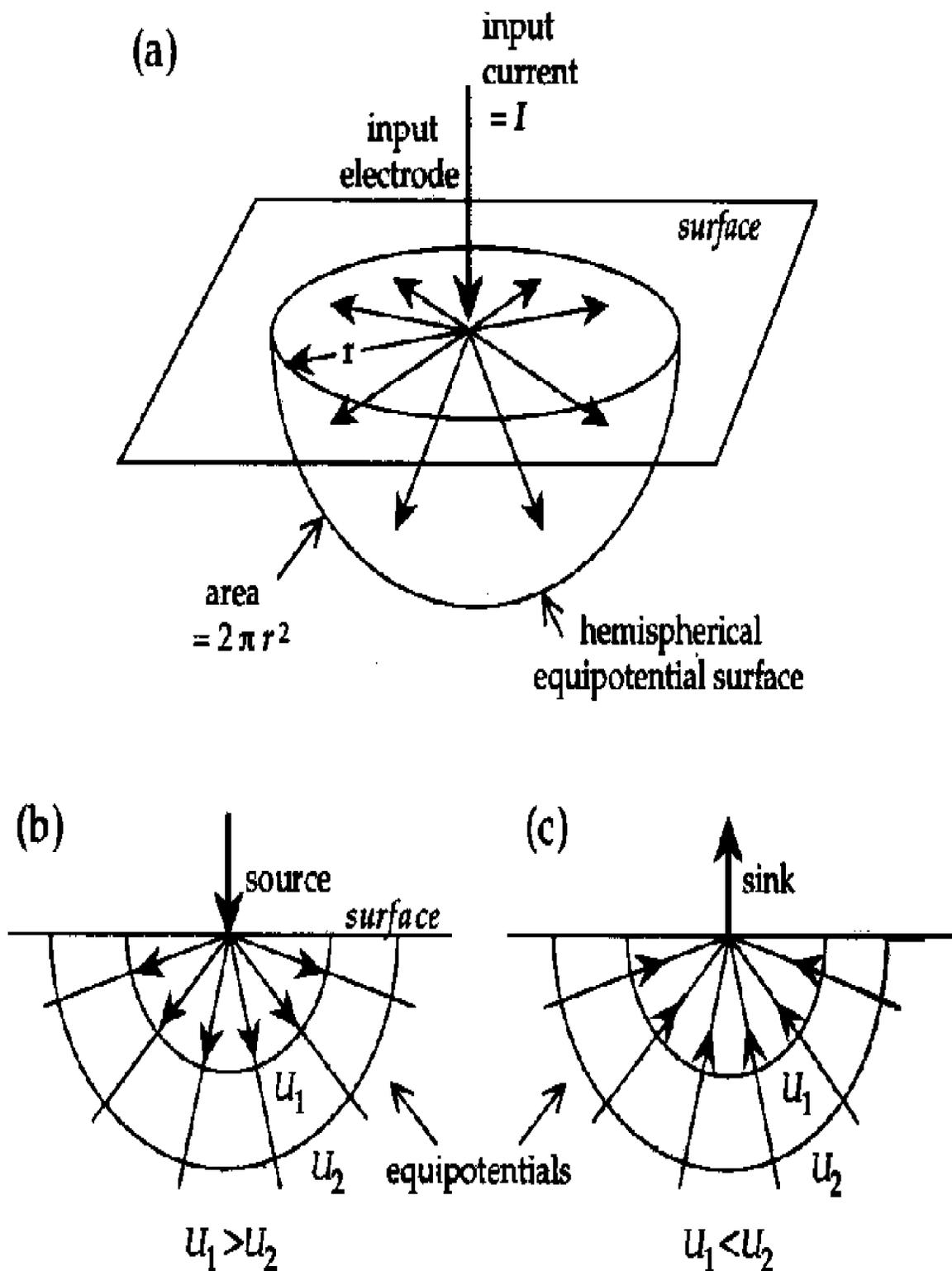
Figure 5.4. Illustration of uniform equipotential surface with current flow lines in all directions (a) and 2-D cross-sections of the hemispherical surfaces at the source (b) and sink (c) electrodes (Lowrie, 1997).
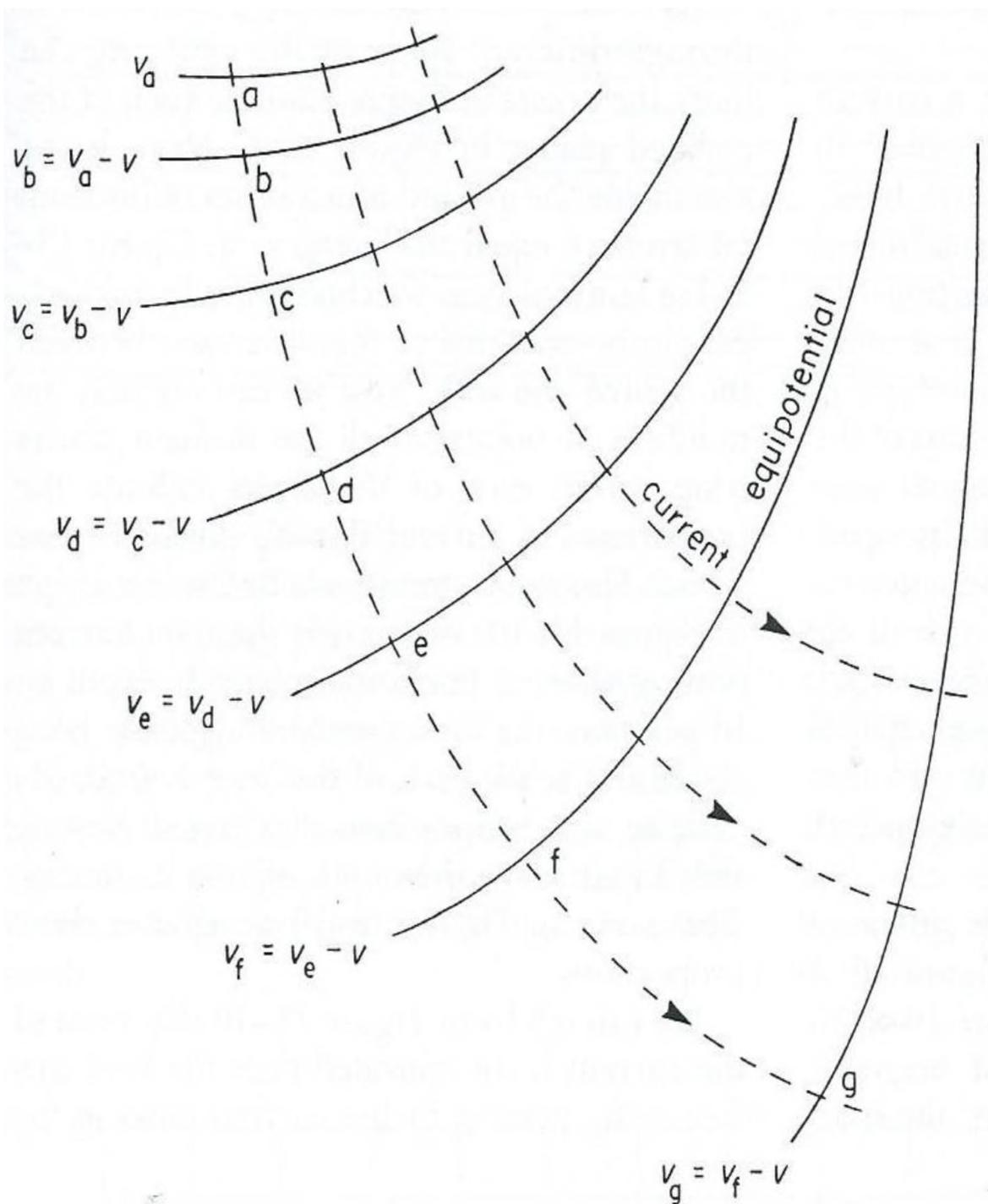
Figure 5.5. Illustration of the change of equal potentials along a current flow line from source/sink (Robinson and Coruh, 1988).
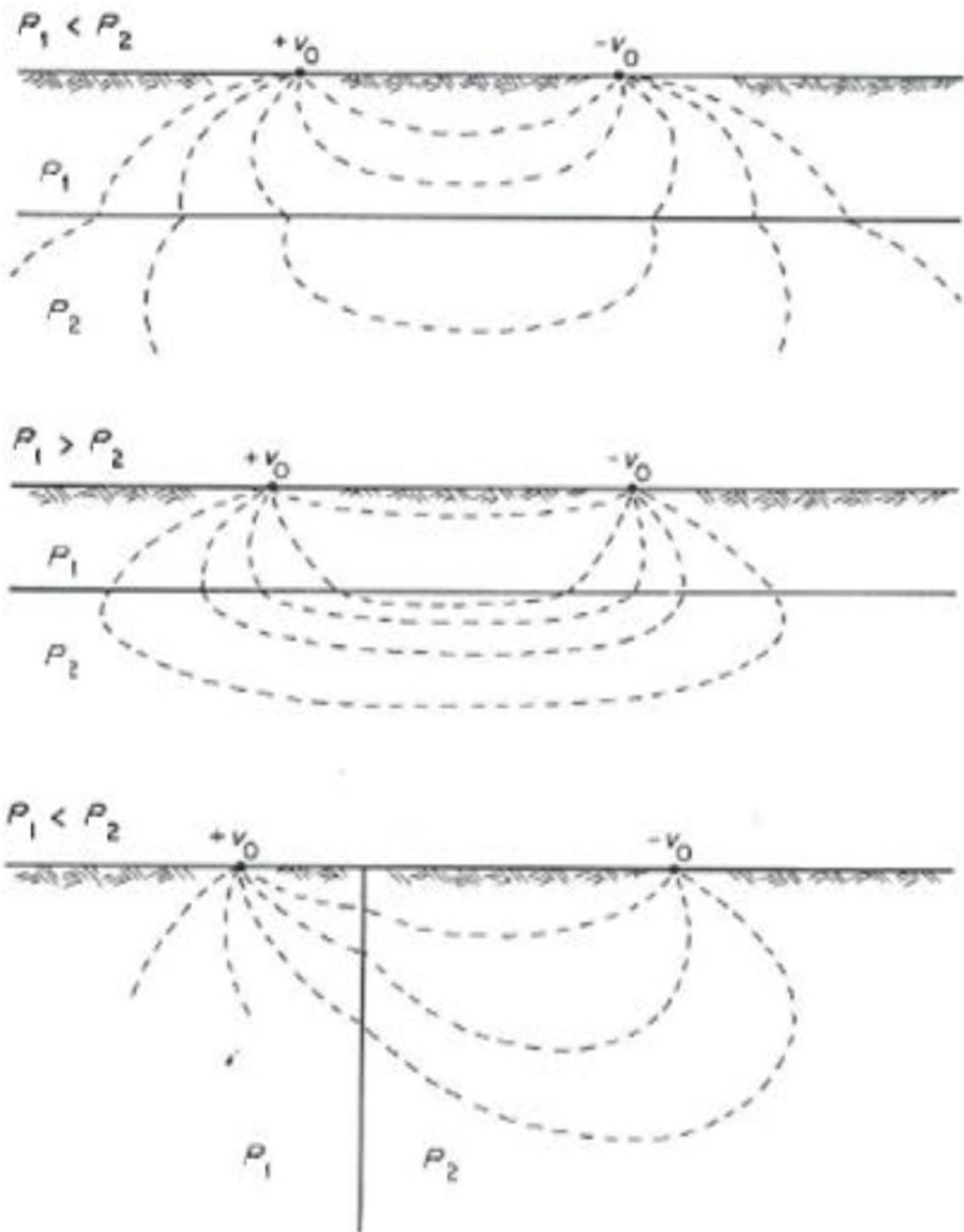
Figure 5.6. Illustrates current flow lines across interfaces with different resistivity (ρ_1, ρ_2) (Robinson and Coruh, 1988).

5.1.4. ERT Data Acquisition. The process of setting up an ERT survey and acquiring data is relatively straight forward. ERT data can be acquired several different ways and depending on the type of investigation may be more advantageous to use one of a variety of electrode array configurations (Figure 5.8). Currently, 2-D and 3-D surveys are more common over the traditional 1-D surveys. 2-D/3-D surveys produce more reliable data because they take into effect lateral variations and provide better resolution and can be performed at relatively low cost. However, array setup can be more time consuming. An ERT survey is usually powered using one or two 12 volt batteries to supply power to the resistivity meter and current to the ground. The resistivity meter commonly used is the automated multi-channel AGI SuperSting R8 unit (Figure 5.7). This unit connects to the switch box and multi-core, active and passive electrode cables and is capable of connecting up to 65,000 interconnected electrodes for one survey. The electrode cables are coupled to metal stakes, usually with rubber bands, which are hammered into the ground. Site conditions may require the addition of water around the metal stakes where the soil is dry or has a high permeability. The electrode cables are arranged along a pre-determined linear traverse and are spaced apart at pre-determined intervals. A pair of electrodes serves as a source and another pair for the sink. A laptop can be used to download the data or upload additional information from the SuperSting R8 unit.

Figure 5.7. The SuperSting R8 unit (right) with 12 volt battery (left) and switchbox (middle) (Ganesh, 2009).

5.1.5. The Dipole-Dipole Array. The dipole-dipole array is one of the most commonly used array types and was used for this study. This array setup is illustrated in Figure 5.8 (e) along with its corresponding geometric constant k. The dipole-dipole array is often used in bedrock studies for imaging karst features, tunnels, and other voids? because it can provide data with good lateral and vertical resolution (Coskun, 2012). This array is also ideal for mapping bedrock with more pronounced vertical changes and features rather than thin horizontal features.

The depth of investigation is controlled by the terms a and n in the geometric factor k (Loke, 1999). The typical depth of investigation for the dipole-dipole array is about one fifth or 20% of the total array length. Another characteristic this array offers is the low E.M. coupling between the current and potential circuits (Loke, 1999). With the dipole-dipole array, the ρ_a values are calculated for all the possible electrode pair combinations and all possible n values. A pseudo-section is then created by plotting all ρ_a values. The ρ_a values are plotted as a function of midpoint and n. Figures 5.9 and 5.10 illustrate this. Other arrays such as the Wenner and Schlumberger array are better for seeing vertical changes (Loke, 1996-2016).
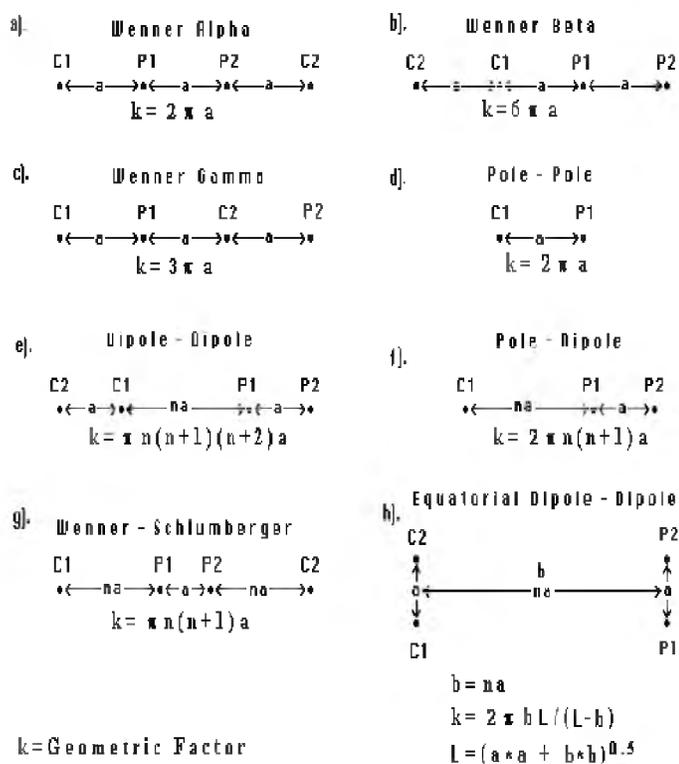
Figure 5.8. Different types of array configurations (Loke, 1999-2016).

2 Dimensional Resistivity Profiling:
Dipole-dipole Array

☐ Electrode Location
◆ Apparent Resistivity Plotting Location
Ⓘ Transmitted Current
Ⓥ Measured Voltage Gradient
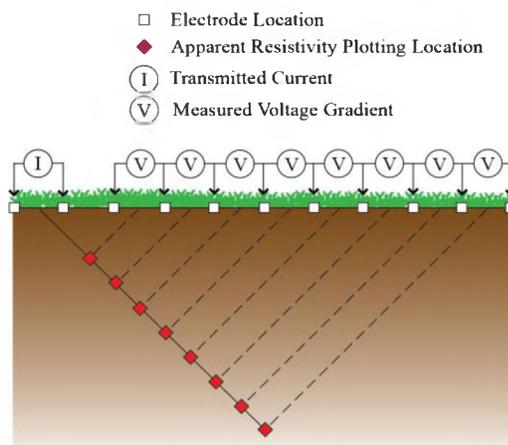
Figure 5.9. Illustration of 2-D Dipole-Dipole array pseudo-section plot.
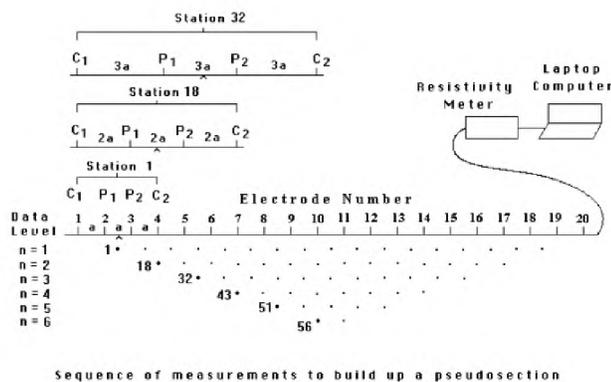
Figure 5.10. Building a pseudo-section (Loke, 1999).

5.1.6. ERT Data Processing. ERT data are processed using the Res2DInv inversion software. The "stg" file that contains the raw data is converted into a ".dat" or data file where topographic points are added. The points are determined from distance and elevation data collected along the ERT traverse. The software reads the data file with set inversion parameters. Before the inversion process is carried out, the software prepares all the ρ_a values in a profile display where data points are inspected and any erroneous data

points are removed. Bad data can be caused by several different factors from poor coupling of electrodes to the metal stakes to poor conduction caused by the lack of moisture in the ground. After erroneous data is removed, the inversion process is performed. The objective of the inversion process is to create a true resistivity profile by minimizing, as much as possible, the root-mean-squared value (RMS) or difference between the calculated and measured ρ_a. According to Loke (1999), the relationship between ρ_a and true resistivity is very complex and because of this, inversion must be carried out by computer program. This process requires multiple iterations to be carried out in order to create the best model with the lowest RMS to create a true resistivity profile (Loke, 1999). This is the iteration error.
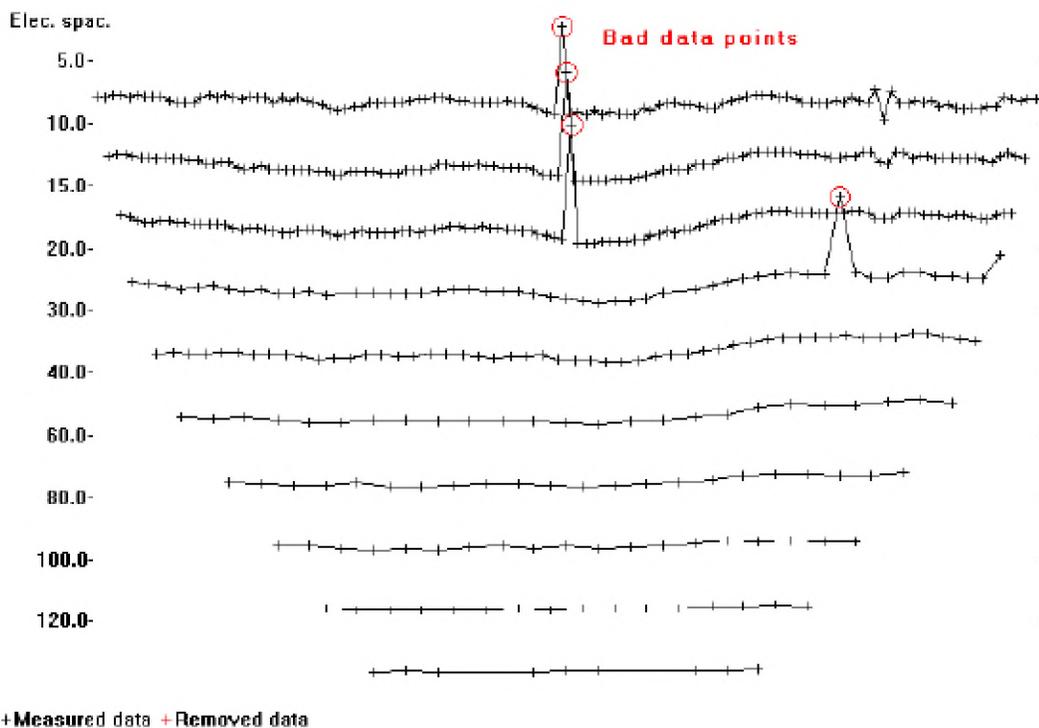
Figure 5.11. Apparent resistivity profile with bad data points (marked with red circles) which need to be removed before the inversion process (Loke, 1999).

5.1.7. Interpretation. In interpretation of the ERT data, known resistivity values of materials are used as shown in Figure 5.12. Interpretation can be extremely accurate when enhanced with ground truth (such as borehole data). Additional factors that can affect resistivity of soil/rock material are temperature, rock type and texture, jointing/fracturing, clay mineralization, and groundwater. Competent, intact rock will have higher resistivity values than highly weathered and fractured rock which can contain more clays and water. Soils with clays, especially moist clay, increase conductivity and will cause much lower values. Clay alteration, dissolution, faulting, and water intrusion also lower resistivity. Faulting and dissolution create conduits for fluid flow that can be replaced with clay minerals from weathering. Induration, precipitation, and metamorphism will also increase resistivity. Figure 5.12 shows a range of resistivity values for common rock types in the study area such as limestone, dolomite, sandstone, and shale. These four rock types can vary from 10 (wet) to 10^4 (dry) ohm meters. Clays can range from 1 to 100 ohm meters while alluvium can range from 10 to 1,000 ohm meters. According to Telford (1990), sand can vary from 1 (wet) to 10,000 (dry) ohm meters and gravels can vary from 100 to 10^4 ohm meters. In Figure 5.01, the contrast between the boundary and more conductive soil and more resistive bedrock is easy to see. Resistivity values jump from about 80 ohm meters to 250 ohm meters in this area. Based on previous studies in Missouri, the typical measured values for moist clays are less than 100 ohm meters; moist soils and heavily fractured limestone rock can range between 100 – 400 ohm meters. Moist soils and bedrock is typically around 125-200 ohm meters. Rock that is mostly intact is greater than 400 ohm meters. This is all dependent on degree of water saturation, porosity, and thickness (Muchaidze, 2008) (Nwokebuihe, 2013).
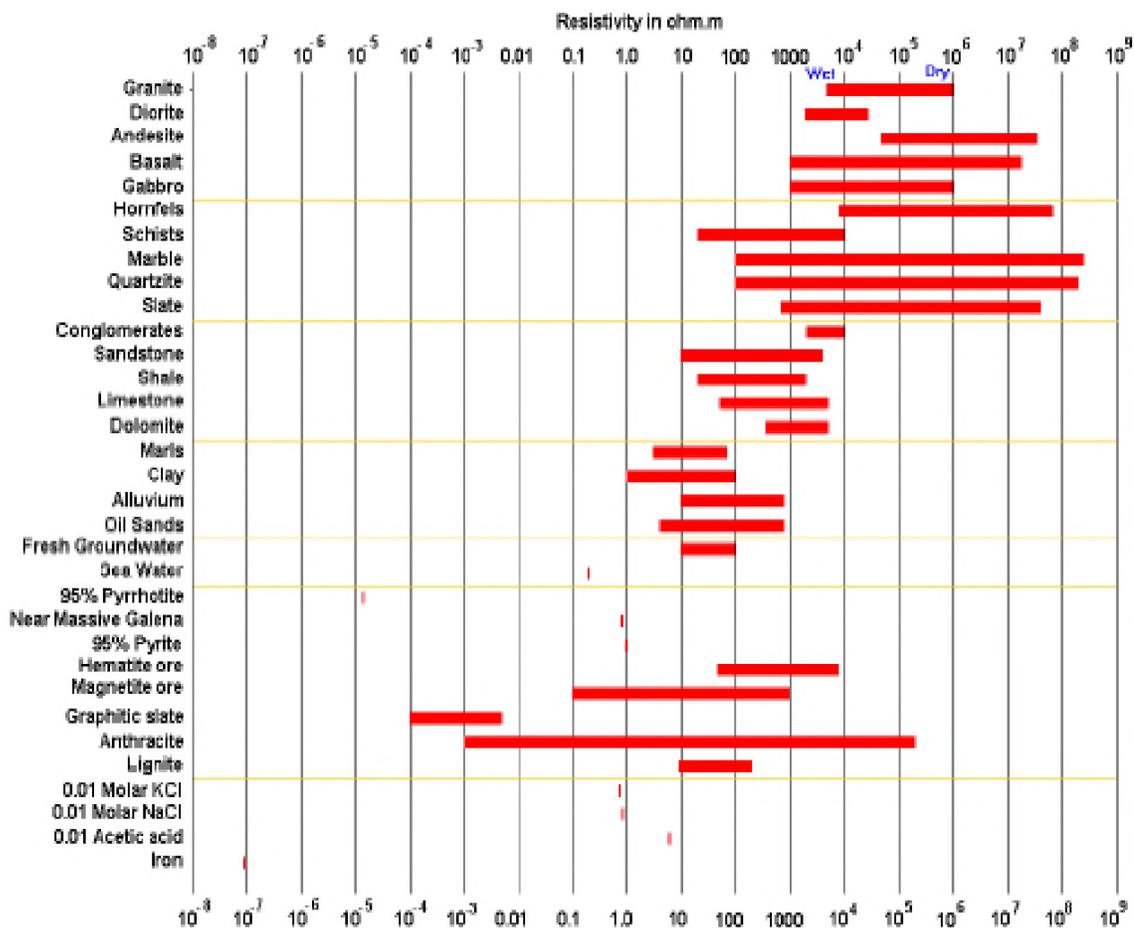
Figure 5.12. Ranges of resistivity for some rocks and minerals
Loke (1996-2016).

5.2. MULTI-CHANNEL ANALYSIS OF SURFACE WAVES (MASW)

Multi-Channel Analysis of Surface Waves (MASW) is a geophysical tool developed by the Kansas Geological Survey that has become commonly employed over the last thirty years. The reason for this is because this tool measures seismic surface waves or ground roll, more specifically, fundamental mode Rayleigh waves. In the past, these waves were only considered as noise and disregarded because techniques to analyze surface wave data had not been developed. Currently, this tool can be used to detect bedrock surfaces, shallow tunnels, abandoned mines, and fracture systems at relatively low

cost (Miller et. al., 1997). MASW surveying is relatively easy and much less time consuming and destructive when compared to other methods such as drilling. A MASW survey can be performed with just two people. Equipment setup, data acquisition, and processing can all be done in about 30 minutes depending on site conditions and data quality. MASW also can work well in acoustically noisy environments. It is not as effective in areas where bedrock depth is highly variable. This geophysical technique can collect active and passive data from a source when using an array of geophones to measure wave travel times and magnitudes. Once the data is collected, it is processed and interpreted using the output 1-D shear wave velocity profile. The shear wave velocity is used to determine the stiffness or rigidity of soil and rock. Interpretations can be very accurate with ground truth constraints such as boreholes. Conventional refraction and reflection seismic surveys collect signals with frequencies greater than 50 Hz at great depth where MASW collects surface waves with frequencies of 30 Hz or less at a shallower depth (Park et. al., 2007).

 5.2.1. Wave Types. Surface waves, like body waves, are generated anytime an acoustic source is created in or on the surface. This source could be from a sledgehammer, explosive, traveling cars, distal earthquakes, etc. These sources produce acoustic energy or strain energy that is propagated through the particles of the surface. This acoustic energy consists of body waves and surface waves. Body waves consist of compressional waves (p-wave) and shear waves (s-wave). P-waves propagate by compressional and dilational strains and S-waves propagate from perpendicular strain (Figure 5.13) (Thitimakorn and Anderson, 2005). The P-wave is governed by the bulk modulus (K), shear modulus (μ), and density of a material. The S-wave is governed by only the shear modulus and material

density. Body waves travel faster than surface waves and are measured in reflection and refraction surveys.
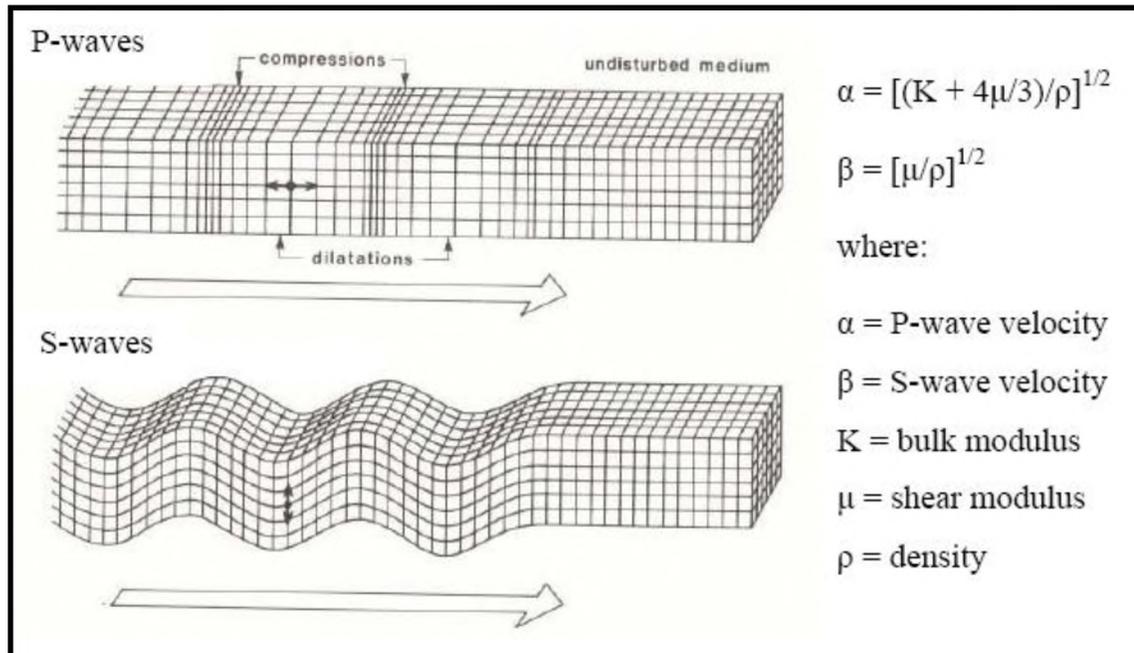
Figure 5.13. Propagation of P-wave and S-wave motion and velocity equations (Thitimakorn and Anderson, 2005).

Surface waves consist of Rayleigh waves and Love waves. Surface waves are horizontally traveling plane waves confined to the shallow subsurface (Park et. al., 2002). Of these two waves, the Love wave is the most destructive when produced from earthquakes because they rupture the ground surface. Love waves are typically not recorded in most seismic surveys. This is due to the horizontal, side to side motion that characterize them. Rayleigh waves are characterized as having horizontal and vertical particle motion. The maximum particle motion or amplitude of Rayleigh waves is achieved at the air-ground interface (Anderson, 2017). Rayleigh waves propagate away from the source in a retrograde or clockwise motion as shown in Figure 5.14. This retrograde motion

is maintained near the surface, however, as depth increases, the motion becomes increasingly prograded (clockwise) (Alsulaimani, 2017). The depth of Rayleigh wave particle motion is a function of the source magnitude and frequency. Larger sources create a larger range of frequencies and larger wavelengths with lower frequencies. Lower frequency particle motion reaches greater depth while higher frequency motion is limited to a shallower depth (Anderson, 2017). Different frequency Rayleigh waves propagate at different velocities, that is, they are dispersive in a heterogeneous environment (Figure 5.15). In heterogeneous media, S-wave and P-wave velocities vary with depth (Thitimakorn and Anderson, 2005). For Rayleigh waves, higher frequencies will have lower phase velocities and lower frequencies will have higher phase velocities. The velocity of these waves is a function of the engineering properties of the media (Thitimakorn and Anderson, 2005). Velocity versus frequency data can be converted to depth versus S-wave velocity (Anderson, 2017).
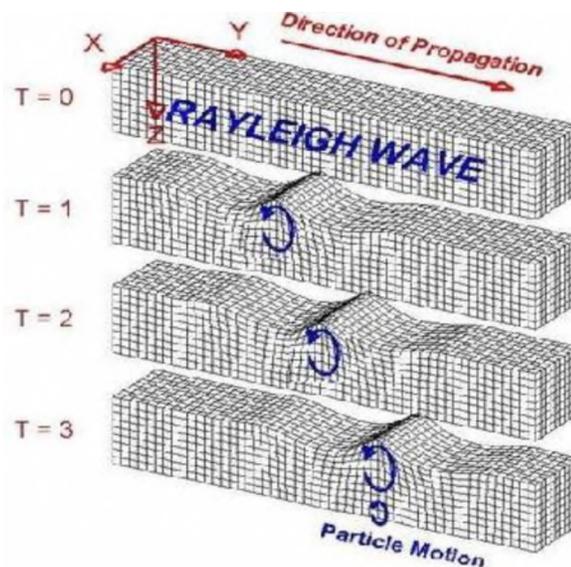
Figure 5.14. Illustrates the propagation of Rayleigh wave motion through the surface with respect to time. (Anderson, 2017).
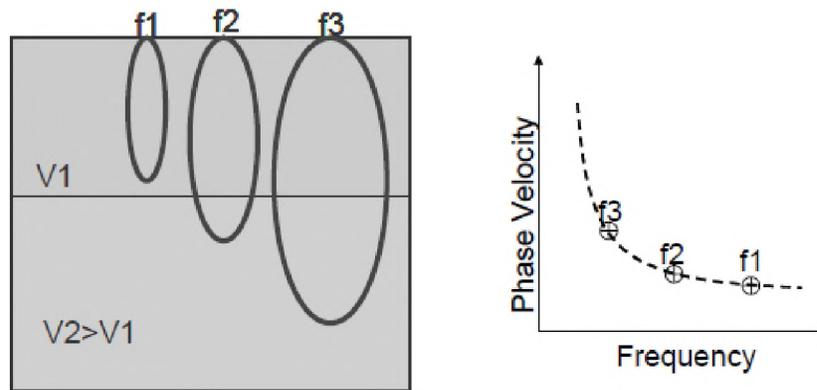
Figure 5.15. Illustration of dispersive components of different frequencies versus velocity (Billington et. al., 2007).

To determine the Rayleigh wave phase velocity, it is assumed that the ground is comprised of a uniform half-space in elastic medium. Because the medium is homogenous, it is non-dispersive and phase velocities are constant. Rayleigh wave velocities are much more dependent on S-wave velocities than those of P-waves, that is, Rayleigh wave velocities are much more sensitive to S-wave variations than P-wave variations. Surface wave velocity varies from about 87% to 96% of the S-wave velocity (Billington et. al., 2007). Rayleigh wave phase velocities can be determined using the equation (Anderson, 2017):

$$V_R^6 - 8\beta^2 V_R^4 + \left(24 - \frac{16\beta^2}{\alpha^2}\right)\beta^4 V_R^2 + 16\left(\frac{\beta^2}{\alpha^2} - 1\right)\beta^6 = 0 \qquad (15)$$

where:

V_R = Rayleigh wave velocity

β = shear wave velocity

α = compressional wave velocity

Since V_R is much more sensitive to β, S-wave velocities are relatively easy to extract. V_R is much more comparable to S-wave velocity. S-wave velocity is a function of the shear modulus and material density. The higher a materials shear modulus, the higher V_S becomes. The shear modulus represents the material strength or rigidity. V_S can be found by the following equation:

$$V_S = \left(\frac{\mu}{\rho}\right)^{\frac{1}{2}} \qquad (16)$$

where:

V_S is the S-wave velocity;

ρ is the material density;

μ is the shear modulus

The shear modulus of a material can be expressed in equation:

$$\mu = \frac{Shearing\ Stress\ \tau}{Shear\ Strain\ \tan\theta} \qquad (17)$$

In a uniform half-space, V_R and V_S are can be related by the equation:

$$\beta = \frac{V_R}{C} \qquad (18)$$

where C is a constant that represents Poisson's ratio (V_P/V_S) for a material. In nearly all situations the variation of C lies somewhere in the range of 0.874 to 0.955. Ultimately, it depends on the site characteristics (Anderson, 2017). A accurate assumption for V_R is expressed in equation 18:

$$\approx 0.9 V_S \qquad (19)$$

In heterogeneous media, V_S is averaged under the entire array and subdivided for each layer. A ten layer model is generated using the average V_S subdivided into each layer.

The average V_S is found by the equation (Anderson, 2017):

$$Avg\ V_S = \sum_{i=1}^{n} d_i \ / \sum_{i=1}^{n} \frac{d_i}{V_{Si}} \tag{20}$$

5.2.2. Data Acquisition MASW data are acquired similarly to other seismic surveys. MASW data can be acquired as passive or active. Passive data does not depend on an active source. Passive data is produced from ambient noise such as road traffic, distal earthquakes, etc. Active data is collected using an impact source, an array of geophones, and a seismograph. An impact source can be a sledgehammer on an aluminum plate, cable drop using cranes, explosives, etc. The geophones are the receivers that measure the propagating Rayleigh waves which are recorded by the seismograph. The receiver number is the channel number. MASW survey equipment and setup, as shown in Figure 5.16 and Figure 5.17 consists of sledgehammer and plate source with an array of geophones and a seismograph. The seismograph is controlled using a laptop and powered by 12V battery. During a survey, the geophones (receivers) are connected to the cable and coupled to the ground. The laptop operator arms a switch that is placed at the base of the plate. When the hammer hits the aluminum plate, the switch activates the Seistronix RAS-24 seismograph and the wave arrival times are recorded. The output data is referred to as a shot gather or record. Multiple shot gathers are usually obtained at each location for stacking.

5.2.3. Field Configuration and Parameters. MASW array configuration is dependent on the site-specific geologic conditions such as soil type, depth, and type of investigation. Different soil/rock types have different shear moduli and therefore different V_S. Unlike intact rock or dry compact soils, highly fractured rock and under-densified soils will have a lower shear modulus and therefore lower V_S. Under-densified soils such those with large amounts of dry, loose sand and gravel can cause problems with generating

acoustic energy due to signal attenuation. The loose soil can act as a muffler to the source (Anderson, 2017). The acquired data is used to characterize the soil and bedrock. These parameters have been debated over recent years and studies are still being conducted to determine what the optimal parameters truly are for recording fundamental mode waves.

For a typical MASW survey (Figure 5.17), 24 geophones recording 4.5 H_Z are used with a source offset (x_i). No less than 8 geophones should be used (Anderson, 2017). The 4.5 H_Z geophones are vertically polarized and cannot record love waves which are horizontally polarized. Any frequencies lower than 4.5 H_Z are filtered out and not recorded. Frequencies up to around 150 H_Z can be recorded. The geophone spacing (dx) is related to the shortest wavelength (λ_{MIN}) and shallowest resolvable depth (Z_{MIN}) (Park and Adkins-Heljeson, 2006):

$$dx \approx \lambda_{MIN} \approx Z_{MIN} \qquad (21)$$

The geophone spacing is typically 2.5 ft or 5 ft intervals. Decreasing the spacing will render higher resolution at shallower depth. Increasing distance will increase depth, but decrease resolution. A rule of thumb for geophone spacing is that the spacing is determined by the smallest layer that can be resolved. An example would be if the geophone spacing is 5 ft, then the smallest layer that can be resolved is about 5 ft. The maximum obtainable depth of investigation is about 100 ft to 115ft depending on site characteristics (Anderson, 2017). It has normally been considered that the total geophone array length (D) is directly related to the longest wavelength (λ_{MAX}) that can be analyzed and determines the maximum depth of investigation (Z_{MAX}). Z_{MAX} is mostly limited by the source since it is the controlling factor (Park and Adkins-Heljeson, 2006). Therefore:

$$D \approx \lambda_{MAX} \approx Z_{MAX} \qquad (22)$$

The offset (x_i) is the distance between the source and geophone. Park and Adkins-Heljeson (2006) suggest an offset value of about 20% - 25% of D. According to Park et. al. (2002), for most common soils, the optimal offset is important for recording fundamental mode Rayleigh waves in the frequency range of 5 H_Z – 50 H_Z and phase velocities of 50 m/sec – 1,000 m/sec. Having an optimal offset distance will help avoid interference from near- field and far-field effects. A longer offset distance x_i and D will increase the effects of higher modes and lower the signal to noise ratio (S/N) for fundamental modes. Higher mode surface waves dampen the fundamental mode waves as offset distance increases. These near-field and far-field effects are still not fully understood due to it being a multi-factored problem (Park and Carnevale, 2010). Park and Adkins-Heljeson (2006) suggests the values x_i = 5 m, dx = 1 m, and D ≤ 30 m to mitigate these effects and recommend a 1dx-12dx interval for source-geophone configuration movement. The interval of 4dx or close to it is commonly used with 24-channel array. The MASW technique has the most tolerance in the selection of optimum field parameters over all other methods because surface waves have the strongest signal to noise ratio (S/N) (Park et. al. 2002).

The recording time or length is also an important parameter. Increasing the recording length too much can result in interference from ambient noise. Excessively decreasing the recording length can result in data dominated by higher mode surface body wave energy. Typically, the recording length is one second with a one millisecond sampling interval. Park and Adkins-Heljeson (2006) recommend a one millisecond interval with a two second total recording length., A longer recording time is best for V_S lower than 100 m/sec.

Figure 5.16. Typical equipment used in MASW surveys. a) Trigger extension, b) RAS-24 Seismograph, c) 12V Battery, d) Trigger, E) Serial cable for laptop, f) Geophones, g) Geophone connection cable, h) Sledgehammer and aluminum plate (Pires et. al., 2019).

Figure 5.17. A typical MASW survey setup with source, seismograph, and geophone (Mohamed et. al, 2013).

5.2.4. MASW Data Processing. After MASW data are acquired, it is then processed using the SurfSies software created by the Kansas Geological survey. The main processing steps consist of pre-processing of records, picking the dispersion curve, and generating a 1-D shear wave velocity profile. During pre-processing, multiple shot gathers from each location are stacked. Stacking is used to suppress ambient noise. The velocities are calculated from the slopes (Δ time/Δ distance) from the field records and later converted. After stacking, muting and filtering is applied to the field data to eliminate all other unnecessary data to focus the dispersion curve on surface waves. Adequate muting will eliminate refraction, reflection, and higher mode surface wave energy. Excessive muting can result in a poor-quality overtone image and therefore a poor dispersion curve. After the pre-processing, a dispersion curve is extracted, and points are picked manually from the generated overtone image. The overtone image displays the intensity of the phase velocity versus frequency. The dispersion curve is the plot of the phase velocity versus frequency data. During this part of the processing, it is important to pick the highest velocity/lowest frequency fundamental mode data correctly to get the best results and least amount of error during inversion. The inversion process is performed to create a 1-D V_S profile. The 1-D V_S profile represents the average V_S under the entire array. Layers subdivided and averaged using equation 20 and a 10-layer model is then produced. The amount of estimated error during the inversion is calculated as the root mean square error (RMS). An RMS of about 5 or lower is best. The idea is to keep it as low as possible.
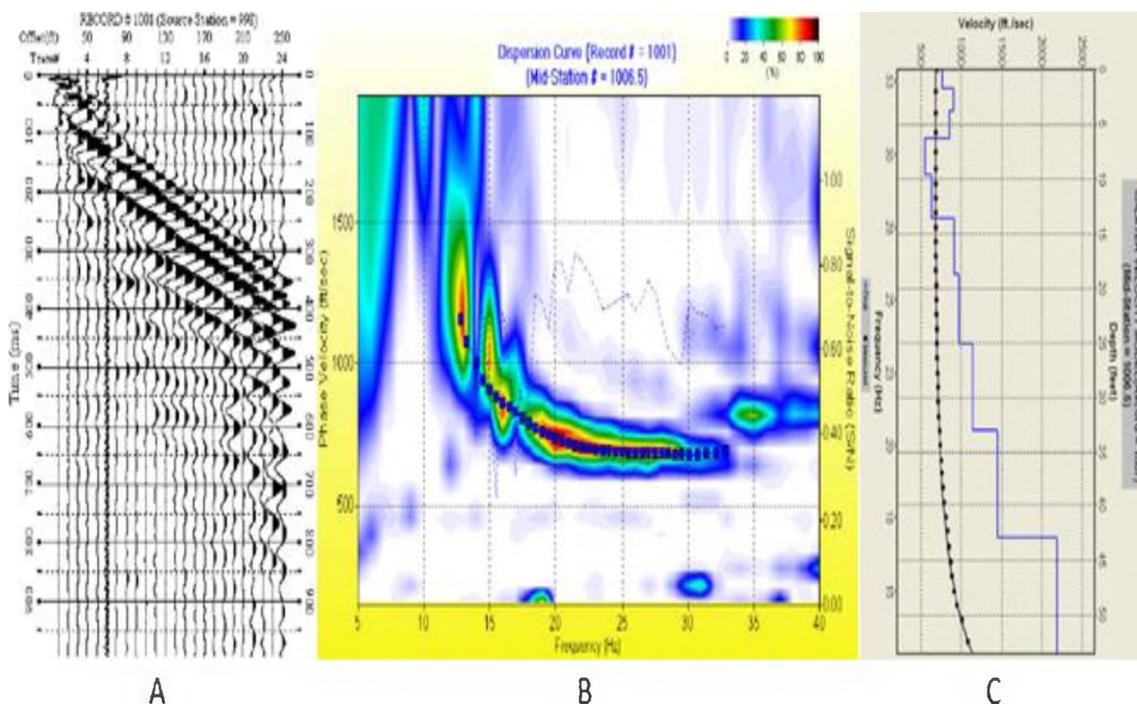
Figure 5.18. Main processing steps using SurfSeis software including: a) a shot gather, b) a picked dispersion curve, and c) 1-D Shear wave velocity profile (Anderson, 2017).

5.2.5. Interpretation. When interpreting MASW data, it is important to remember that the V_S data is averaged under the entire array (Anderson, 2017). It does not represent what is under each receiver. The 1-D shear wave velocity profile represents this average and is referenced at the midpoint of the geophone array. For a 24-channel array, the midpoint would be between receivers 12 and 13. Interpreting MASW data works best when the data can be enhanced with ground truth. Borehole data can help confirm bedrock depth and soil conditions when looking at the 1-D V_S profile. Site conditions such as irregular topography and sharp changes in the subsurface can make interpretation difficult. Figure 5.19 shows the National Earthquake Hazard Reduction Program (NEHRP) classification. This chart was designed to classify a site per the International Building Code based on the V_S of different materials present. Sites with weaker soils and fractured

bedrock will have lower V_S and higher signal attenuation than sites with very stiff soils and hard, competent bedrock. Typical bedrock for Missouri is limestone and based on previous studies, V_S for limestone has been found to around 1,000 ft/sec for heavily weathered limestone to 1,200 ft/sec or greater for more competent limestone bedrock. Figure 5.19 classifies soft soil profiles at approximately 600 ft/sec or less; stiff soil profiles between 600 ft/sec to 1,200 ft/sec; and very dense soil and soft rock between 1,200 ft/sec to 2,500 ft/sec.

Site Class	Soil Profile Name	Average Properties in Top 100 feet (as per 2000 IBC section 1615.1.5) Soil Shear Wave Velocity, V_S	
		Feet/second	Meters/second
A	Hard Rock	$V_S > 5000$	$V_S > 1524$
B	Rock	$2500 < V_S \leq 5000$	$762 < V_S \leq 1524$
C	Very dense soil and soft rock	$1200 < V_S \leq 2500$	$366 < V_S \leq 762$
D	Stiff soil profile	$600 < V_S \leq 1200$	$183 < V_S \leq 366$
E	Soft soil profile	$V_S < 600$	$V_S < 183$

Figure 5.19. National Earthquake Hazard Reduction Program (NEHRP) site classification.

6. CASE STUDY

A detailed discussion of the geophysical investigation is given in this section. It includes an overview of the study followed by a brief description of the study site, geophysical surveys, and interpretation of the survey results.

6.1. OVERVIEW

To mitigate sewage contamination during flooding, a small municipality has planned to establish a series of tunnels to connect wastewater to sewage plants. The tunnels would not only serve as reservoirs, but also as a means to discharge wastewater and sewage to and from neighboring facilities. These tunnels would help prevent sewage backup into nearby residences and businesses and prevent contamination of the Meramec River during periods of flooding. The goal of the investigation was to conduct geophysical surveys of the proposed tunnel locations to determine the depth to bedrock beneath the Meramec River and identify any anomalous zones below the 300 ft elevation mark that may need to be addressed.

In this investigation, land/marine ERT and MASW surveys were conducted along with echo-sounding (ES), side-scan sonar (SSS), and sub-bottom profiling (SBP). Multiple soil borings taken near the area were used for ground truth and used to aid in data interpretation.

6.2. STUDY SITE

The study area is located in St. Louis County, Missouri in the Meramec River Valley. The proposed tunnel locations extended from west to east and crossed the river. Geophysical surveys were performed along a traverse near the proposed location. Multiple MASW surveys were performed along both riverbanks and an ERT survey was performed that spanned across the river (Figure 6.1). Boreholes for the project were acquired on both sides of the river prior to the geophysical investigation. These boreholes were used to provide ground truth for aid in interpretation. The soil at the site has been previously characterized as Holocene alluvium that can range in thickness from 0 to 215 ft that is underlain by the Warsaw Formation and Keokuk Limestone. A geologic map of this location from (Harrison, 1997) is shown in Figure 6.2. Three different formations are present in the immediate area: the Salem Formation (Ms), the Warsaw Formation (Mw), and the Keokuk and Burlington Limestones (Mkb). River fill materials consist of Holocene and Pleistocene age terrace deposits and Holocene age alluvium. Both are comprised of gravel, sand, silt, and clay.
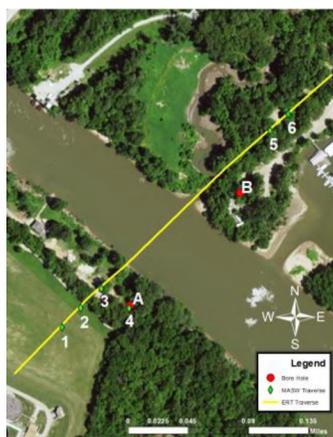
Figure 6.1. Aerial photo of the site with ERT survey traverse, MASW locations, and boreholes shown.
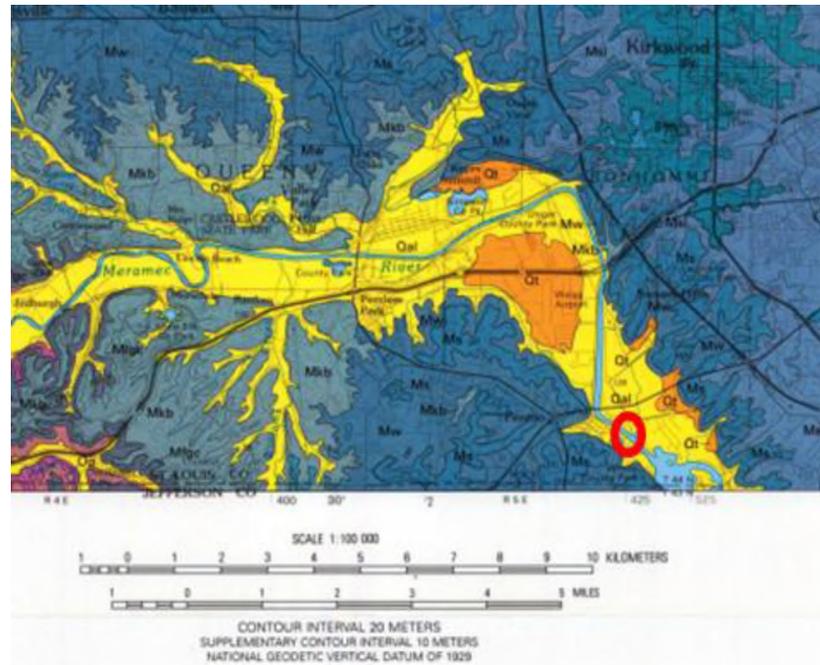
Figure 6.2. Geologic map of bedrock in the St. Louis County area and site location (red circle) (Harrison, 1997).

6.3. GEOPHYSICAL STUDY

The geophysical field portion of the study was conducted over a two day period on October 10th and 11th of 2016. Electrical Resistivity Tomography (ERT) and Multi-Channel Analysis of Surface Waves (MASW) methods were used. Echo Sounding (ES), Side-Scan Sonar (SSS), and Sub-Bottom Profiling (SBP) data were acquired. Two boreholes were installed prior to the study. Additional borehole data from past reports were also examined to possibly help constrain the geophysical data.

6.3.1. Borehole Data. Multiple borehole data have been acquired at the site and elsewhere in the nearby area. Borehole data from the MDNR database and multiple reports were examined to possibly further constrain the data to determine depth to bedrock. Soil samples from two boreholes installed using a split-spoon sampler were collected. One

borehole was installed on each side of the Maremec River. One sample log from borehole A was used in this investigation. MDNR well log data from 4 sites within one mile of the site were also examined as well as test borings from the MDNR WR30 report. Multiple test borings were made upstream and downstream in various locations and two cross-sections were created using the test boring data. The split-spoon sample locations, MDNR well logs, test boring logs found in report WR30, and cross-sections A-A' and B-B' from WR30 are shown in Figure 6.3. Borehole A is located about 100 ft southeast of ERT station 505. The boring log is presented in Table 6.1.

Table 6.1. Borehole A.

Depth (ft)	Soil Description
0-13	Very loose, brown, well graded fine sand; moist.
13-25	Medium dense, brown, poorly graded gravel with sand; moist.
25-33	Medium dense, brown, poorly graded gravel; wet.
33-38	Medium dense, brown, poorly graded sand with clay and gravel; wet.
38-43	Very stiff, red-brown, fat clay with gravel; moist.
43-48	Very stiff, brown, gravelly fat clay; moist.
48-51	Dense, gray, poorly graded gravel with clay; wet
51	Boring terminated

The test boring from MDNR WR30 (44-5-35bba) is located approximately 2,500 ft upstream on the northeast side of the river valley and is the nearest well log to the study area. The surface elevation of the test boring site was 410 ft, very close to the elevations at the study site. Bedrock was encountered at 58 ft. The boring log for 44-5-35bba is presented in Table 6.2. Other nearby test borings from WR30 report very similar depths and were used to create cross-sections upstream and downstream of the study area.

Table 6.2. Test boring 44-5-35bba.

Depth (ft)	Soil Description
0-2	Clay, silty, dark brown
2-7	Clay, sandy, silty, dark brown
7-12	Medium sand, clayey, brown
12-17	Medium sand, silty, brown with gravel
17-22	Fine to medium sand, clayey with gravel
22-32	Medium sand, clayey with gravel
32-58	Medium to coarse sand, clayey, with much gravel
58	Terminated, bedrock
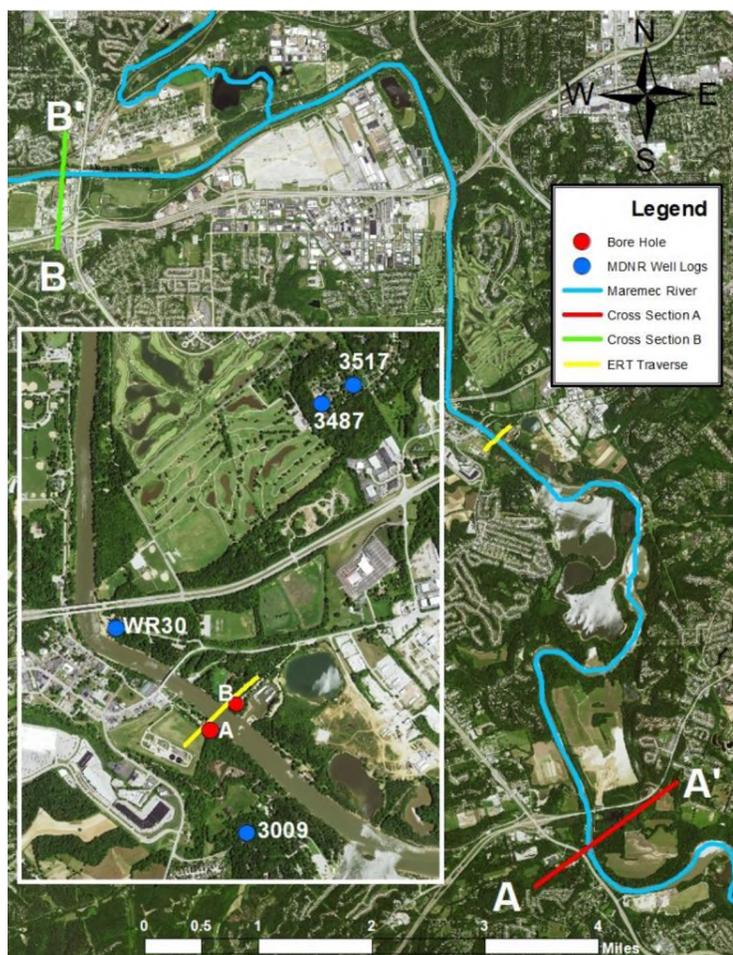
Figure 6.3. Aerial image of the study area showing approximate traverse, borehole, and cross-section locations.

Cross-sections B-B' (upstream) and A-A' (downstream) are shown in Figure 6.4. Cross-section B-B' is approximately 6.8 miles upstream of the study area and cross-section A-A' is approximately 6.4 miles downstream. The study area is about halfway between the two cross-sections. Solid vertical lines represent the various test borings made in the area of B-B'. The soil and bedrock are represented by the numbers 1-6 in these cross-sections. Clay (1), silt (2), sand (3), sand with some gravel (4), sand and gravel in equal amounts (5), and bedrock (6). The bedrock elevation in cross-section B-B' ranges from approximately 346 ft to 380 ft beneath the alluvium. The test borings in B-B' nearest the river show bedrock at 63 ft (left upstream side) and 58 ft (right upstream side). In cross-section A-A', bedrock elevation ranges from approximately 323 ft to 358 ft beneath the alluvium. The test borings in A-A' nearest the river show bedrock at 76 ft (left upstream side) and 75 ft (right upstream side). Prorating the lowest bedrock elevations in the cross-sections with the near equal distances from the study area, the bedrock elevation is estimated to be around 335 ft.
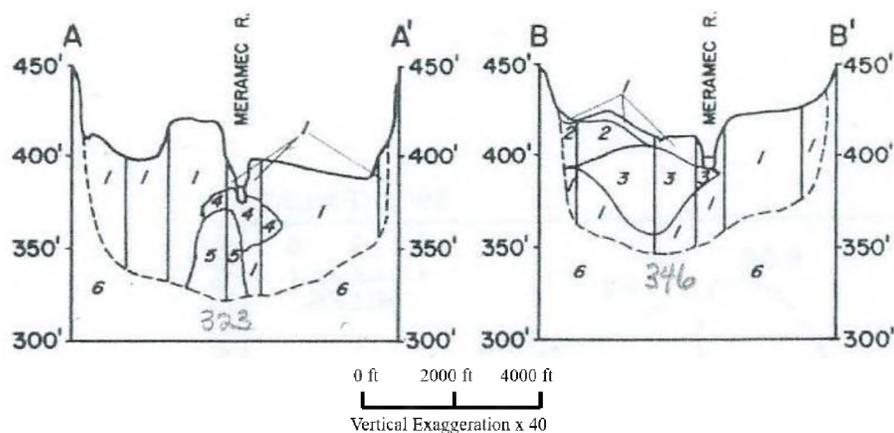
Figure 6.4. Cross-sections A-A' and B-B' oriented looking upstream. Lithology and bedrock depth determined from multiple boreholes obtained throughout the Maremec River Valley (MDNR WR30).

MDNR well logs 3009, 3487, and 3517 were nearest to the study area and examined to help determine bedrock depth and lithology beneath the Maremec River. These well logs are shown in Figure 6.5, 6.6, and 6.7. Using the surface elevation at each well log location, the elevations of the formation top and bottom could be determined. The elevations of top and bottom of the Warsaw formation at well log 3517 is at 460 ft and 360 ft. Well log 3487, the Warsaw formation top and bottom are at 440 ft and 365 ft. Well log 3009, the Warsaw formation top and bottom are at 451 ft and 376 ft. Analyzing the data from the MDNR well logs and the test borings in the cross-sections from the WR30 report, it is likely that the bottom of the river channel is cut into the top of the Keokuk limestone.

Figure 6.5. MDNR well log 3009.

Figure 6.6. MDNR well log 3487.
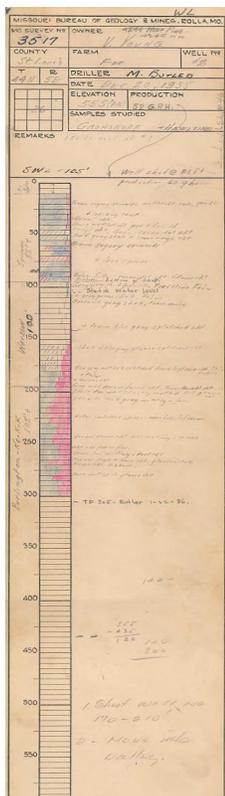
Figure 6.7. MDNR well log 3517.

6.3.2. ES, SSS, SBP Data. Prior to geophysical surveying, bathymetry data were collected on the Meramec River using a boat equipped with ES, SSS, and SBP equipment. These data were collected from an approximately 2,000 ft stretch of river—upstream, downstream, and over the traverse location The ES and SSS data were collected to determine the variable water depth and to image the river bottom. The SBP data were collected to determine the variable depth to bedrock. The ES and SSS provided good quality data that were clear and easy to interpret. The SBP provided poor quality data and the depth to bedrock was unidentifiable. These data were collected for several reasons: to identify any structures that could snag the electrode cable; as well as image any potential features of interest with respect to the proposed tunnel location; and to collect elevation points for the marine ERT portion for processing. No problematic features that could entangle the cable were present.

6.3.3. ERT Survey. ERT data were acquired along a near-linear traverse of 1,670 ft that spanned across the river onto both banks (Figure 6.1). The data were acquired and processed as discussed in section 5 with an AGI SuperSting R8 multi-channel resistivity meter. The ideal electrode array for this project was pre-determined to be the dipole-dipole array. Because of site conditions, two dipole-dipole arrays were overlapped. Each array utilized a total of 112 electrodes consisting of 56 land electrodes and 56 marine electrodes. The electrodes were spaced at 10 ft intervals. The land electrodes were coupled to metal stakes using rubber bands and hammered into the ground. The marine electrodes did not require steaks. Instead, sandbags were fastened to the cable for added weight to ensure the cable would be held to the river bottom. An electric winch was used to keep the cable

somewhat taut in the current. The ERT data were processed using the Res2DInv inversion software.

6.3.4. MASW Survey. MASW data were acquired along the ERT traverse at pre-determined locations on the both riverbanks as shown in Figure 6.1. MASW data were acquired at nine locations along the ERT traverse with one near borehole A. The arrays were orientated both northeast – southwest and then southwest – northeast with the exception of the one MASW survey near A which was oriented south – north and north – south. Three shot-gathers were obtained for each record for vertical stacking. The MASW surveys were conducted using a 24-channel array with 4.5 H_Z geophones spaced at 5 ft intervals. The source was a 12-lb sledgehammer and an aluminum plate. The source offset distance was at 25 ft. The data were processed as discussed earlier in section 5; using the SurfSeis 4 software to produce 1-D shear wave velocity profiles for each location. The stacked data were muted to eliminate noise and the dispersion curves were carefully picked. However, only six locations provided good quality data and therefore only six 1-D shear wave velocity profiles were used in this study. MASW traverses 1, 2, 3, 5, and 6 were centered at ERT stations 215, 315, 415, 1350, and 1425 respectively. Traverse 4 near borehole A is at station 505.

6.4. INTERPRETATION

In this section, interpretation of the ERT and MASW data will be discussed. ERT and MASW data will be compared.

6.4.1. ERT Interpretation. The ERT data were processed and the resulting minimal iteration error was 2.4. This means that the difference between the apparent

resistivity and the true resistivity is low and the processed data correlates well with the measured field data. As discussed in section 5, moist soils and moist, weathered limestone rock can have a resistivity value range of about 100-400 ohm meters but is typically around 125-200-ohm meters. Dry soils with no clay present can be much greater than 125-200-ohm meters. The resistivity will generally increase as the rock competency increases and the moisture content decreases. Porous, fractured rock containing water and piped clay can have resistivity values lower than 125-ohm meters (Anderson and Torgashov, 2017). The interpreted pseudo-section is shown in Figure 6.8.

The interpreted top-of-rock was superposed (black line) at ~200-ohm meters. This was based on the typical resistivity values for limestone, presence of wet clay/gravel, and because borehole B had split spoon refusal at 78 ft which falls on ~200-ohm meters. From the interpretation, depth to bedrock ranges from 10 ft (station 630) to 75 ft (station 1280). The soil is characterized mainly by resistivity values around 50 ohm meters and has values ranging from 10-200-ohm meters.

There are several interesting features in Figure 6.8. There appears to be a paleo-channel beneath station 1 and station 560. A lower resistivity zone of ~250-ohm meters is in the bedrock below station 1050. This could be due to increased moisture content due to fractures, but it does not appear to be piped clay based on the resistivity values. The most interesting features are the two anomalies beneath station 1440. The high resistivity anomaly is characterized by values of 1,500 ohm meters. This higher value indicates that this feature is has a low moisture content and little to no clay and is likely gravels or fill material. The feature begins at station 1320 and continues to the end of the ERT traverse at station 1670. The reasoning for this interpretation is that this section of the ERT traverse

ran along an older gravel/paved parking area. This area can be seen in Figure 6.1. Directly below this feature is a low resistivity anomaly located between station 1420 and station 1550 that can be characterized by values of 50 ohm meters or less. Clay minerals are characterized by values of 100 ohm meters or less and could be the cause of this anomaly. This feature could be formed from karst activity or part of a paleo-river channel. One interpretation of this feature is that it could be caused by a combination of increased water content and clay infilling or piping due to the limestone bedrock being intensely fractured and because the bedrock elevation is actually lower than 300 ft. Another possible interpretation of this feature is that the top of bedrock is at an elevation of about 335 ft. This would be consistent with the data from the WR30 report. However, this anomaly was not reliably imaged. It is possible that this feature was the result of an end of profile anomaly. According to Anderson and Torgashov 2017, end-of-profile anomalies commonly occur.
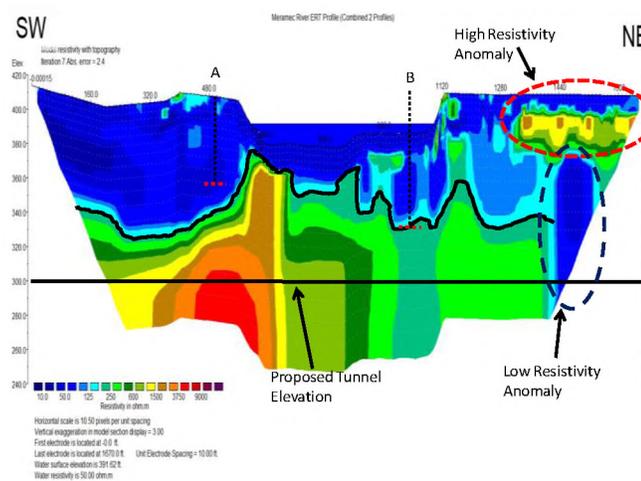

Figure 6.8. ERT pseudo-section with interpreted top-of-rock (black line), MASW profile locations, and anomalies.

6.4.2. MASW Interpretation. Six output 1-D shear wave profiles are shown in Figure 6.9, 6.10, 6.11, 6.12, 6.13, and 6.14 below. The interpreted depth to bedrock is noted in each profile with a red line where Rayleigh wave frequencies first reach 1,200 ft/sec. Based on the NEHRP classification discussed in section 5, the shear wave velocity of limestone bedrock in Missouri is typically around 1,200 ft/sec or greater and was the basis for interpreting the depth to bedrock. Shear wave velocity is dependent on the competency or rigidity of the bedrock as discussed earlier. Heavily weathered and fractured bedrock will have slower shear wave velocities than unfractured, competent bedrock. Shear wave velocities increase as the rigidity of the bedrock increases. The rigidity will generally increase with depth. The interpreted depth to bedrock ranges from 56 ft to 73 ft. The changes in the soil stiffness can be seen in each of the 1-D shear wave velocity profiles as depth increases and shear wave velocity increase to 1,200 ft/sec.
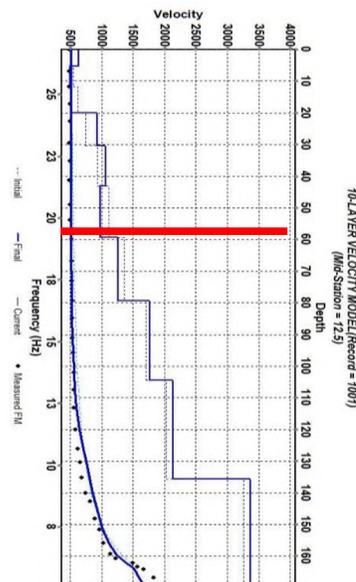
Figure 6.9. 1-D shear wave velocity profile at MASW traverse 1. Depth to bedrock is interpreted to be at approximately 59 ft shown by the red line.
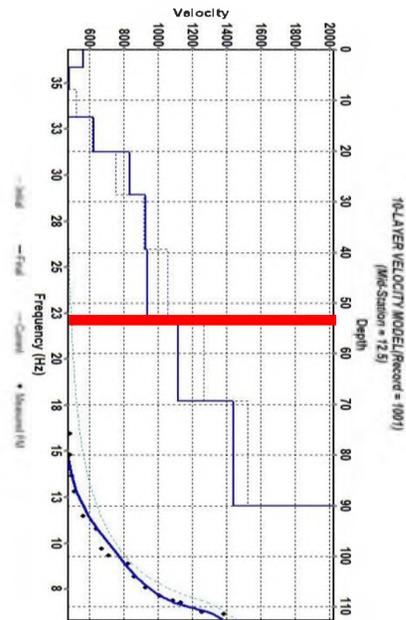
Figure 6.10. 1-D shear wave velocity profile at MASW traverse 2. Depth to bedrock is interpreted to be at approximately 69 ft shown by the red line.
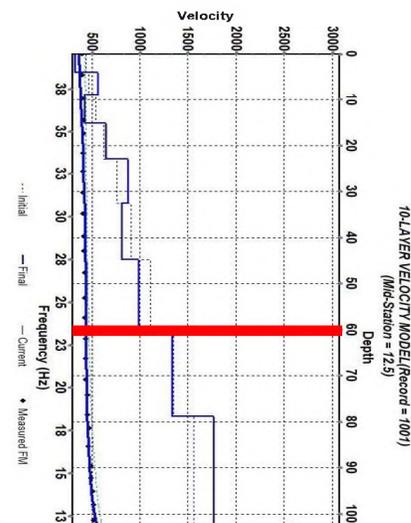
Figure 6.11. 1-D shear wave velocity profile at MASW traverse 3. Depth to bedrock is interpreted to be at approximately 60 ft shown by the red line.
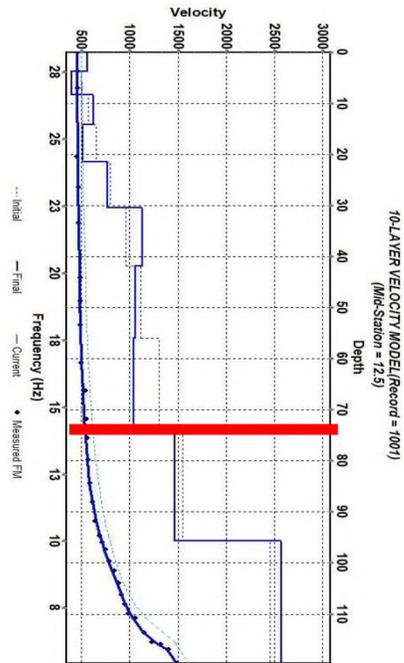
Figure 6.12. 1-D shear wave velocity profile at MASW traverse 4. Depth to bedrock is interpreted to be at approximately 73 ft shown by the red line.
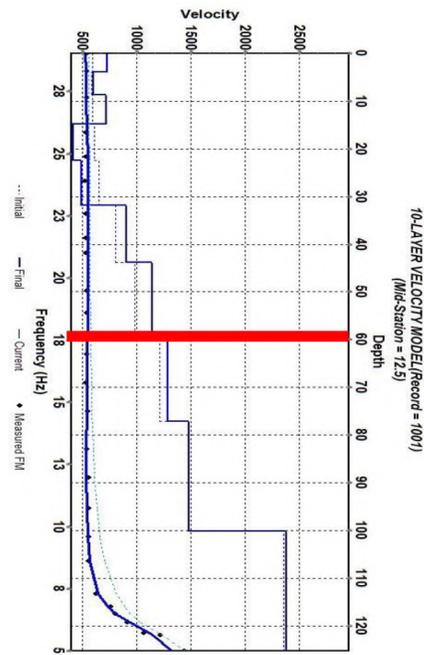

Figure 6.13. 1-D shear wave velocity profile at MASW traverse 5. Depth to bedrock is interpreted to be at approximately 58 ft shown by the red line.
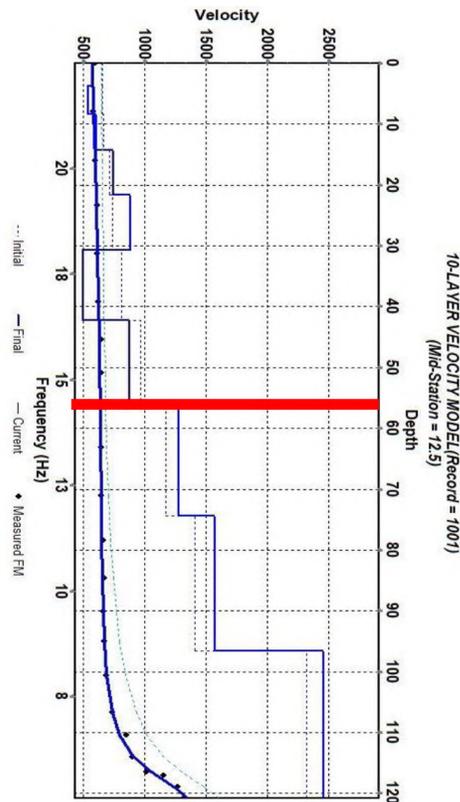
Figure 6.14. 1-D shear wave velocity profile at MASW traverse 6. Depth to bedrock is interpreted to be at approximately 56 ft shown by the red line.

Figure 6.15 shows the combined interpreted ERT and MASW data along with the boreholes A and B. The solid black line along the 200-ohm meter contour marks the ERT top of rock. The MASW traverses 1-6 are shown by vertical solid black lines that show traverse location on along the ERT traverse. The interpreted MASW depth to bedrock is shown by the solid red lines. The locations of boreholes A and B are shown with a dashed black line and the depths of termination are shown with a dashed red line. It can be easily seen that MASW traverses 1, 2 and 4 correlate well and are less than 10 ft within the

interpreted ERT top of bedrock. MASW traverse 3, 5, and 6 do not correlate as well and are within 15 ft or less of the ERT top of bedrock. MASW traverse 3 and borehole A terminate at 65 ft and 51 ft near the 50 ohm meter contour. Dense, gray, poorly graded gravel with clay was logged in borehole A just before termination. Traverse 3 and Borehole A are both within approximately 15 ft of the ERT determined top of bedrock. A dense gravel deposit could possibly be the cause for interpreted shallower depths while the presence of water and clay lowered the resistivity below 50 ohm meters. MASW traverses 5 and 6 terminate at 58 ft and 56 ft and are 15 ft and 20 ft from ERT determined top of bedrock and terminate within the 88 ohm meter - 125 ohm meter contours. These slightly larger resistivity values, 88 ohm meter - 125 ohm meter contours beneath ERT stations 1220 and 1420 are likely caused by the high resistivity anomaly situated in relatively close proximity above the ERT top of bedrock. The soil is likely moist, medium dense, poorly graded gravel with sand as recorded in borehole A log. The data quality for traverses 5 and 6 was slightly lower than traverses 1-4 and more difficult to process. This could be one reason that shear wave velocities were shown to first exceed 1,200 ft/sec at a depth of 58 ft and 56 ft. Another reason is that it could be a similar situation as with traverse 3 or, on the other hand, that bedrock is really 15 ft shallower than the interpreted depth beneath ERT stations 1330 and 1420. The high resistivity anomaly does appear to be shown in the 1-D profile for traverse 6 at a depth of 14 ft to 30 ft which closely matches with the ERT image, however, this feature is not apparent in the 1-D profile for traverse 5. Whether or not the low resistivity anomaly is real or that the depth to bedrock does in fact extend to a depth below the 300 ft mark could not be determined. The 1-D shear wave velocity profile for traverse 6 did not show the bedrock to exceed a depth of 56 ft or an elevation 354 ft.

Further investigation should be conducted to verify the existence and/or the extent of the low resistivity anomaly.
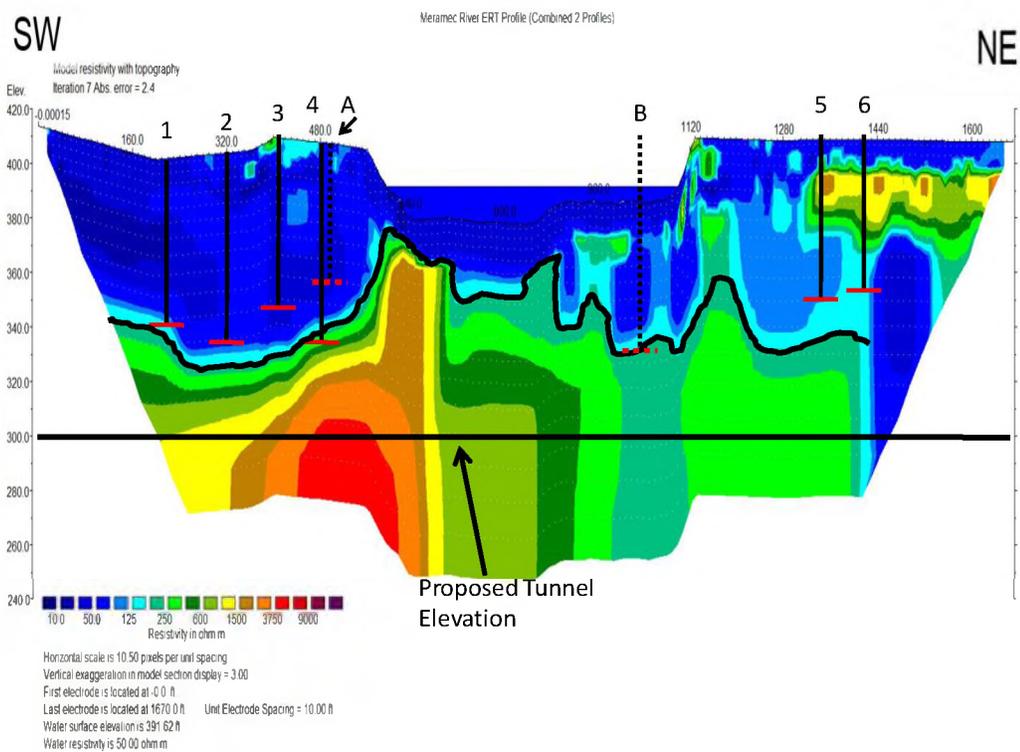

Figure 6.15. Interpreted ERT pseudo-section with interpreted MASW data and boreholes A and B.

7. CONCLUSION AND RECOMMENDATIONS

The ERT and MASW data, along with the borehole data collected at the study site and surrounding area used as ground truth, helped to effectively image the subsurface and determine the variable depth and elevation of the bedrock. The average elevation of the bedrock is 335 ft and can be seen in the interpreted data. This is consistent with the depth determined using the cross-sectional data from the WR30 report. The bedrock in the Maremec River Valley, based on the determined depth/elevation from interpretation and available well logs, is likely the Keokuk limestone rather than the Warsaw formation. The results from of this study show that using ERT and MASW data combined with borehole control can be a very effective way to determine bedrock depth and lithology at a relatively low cost.

The subsurface is characterized by less resistive soils with moist, sand and gravel with clay less than 125 ohm meters. High and low resistivity anomalies were imaged in the soil and bedrock with resistivity values exceeding 1,500 ohm meters and values less than 50 ohm meters. The subsurface was imaged to a depth of 150 ft and elevation of 270 ft, 30 ft below the proposed tunnel elevation. The bedrock beneath the ERT traverse does not appear to contain any fractures or solution-widened joints where clay has been infilled or piped. The bedrock does appear to be competent beneath stations 115 – 600 based on the higher resistivity values. This could pose a problem for tunnel boring machine because the tunnel boring bits would have to be changed before and after encountering this area. However, the anomaly at the northeast end of the ERT profile indicates a potential karst

feature that extends down into the bedrock below a depth of 300 ft and appears to have been infilled with materials containing clay.

Further investigation just upstream and downstream of the study area is recommended along with additional ERT and MASW surveying on the northeast side of the riverbank. Additional surveying could verify whether the low resistivity anomaly near ERT station 1440 is real and if the feature extends to a depth less than 300 ft. Surveying upstream and downstream of the study area could help determine the extent of the feature and whether or not it is present throughout the area and if it is an older river channel or the result of karst activity.

BIBLIOGRAPHY

1. Alshareef, I. F. (2019). *Using the ERT Method to Differentiate Resistivity Anomalies Attributed to Natural and Man-made Activities* (Master's thesis). Retrieved from Missouri S&T Summon.

2. Alsulaimani, Ghassan, Salem. (2017). "Acquisition of active multichannel analysis of surface waves (MASW) data in karst terrain" Doctoral Dissertations. 2735. http://scholarsmine.mst.edu/doctoral_dissertations/2735

3. Alsulaimani, Ghassan Salem, "Comparison of core control and geophysical investigations, silica sand deposits, Dawmat Al Jandal, AlJawf at Saudi Arabia" (2014).*Masters Theses*. 7260.http://scholarsmine.mst.edu/masters_theses/7260

4. Anderson, Neil. (2014)"Chapter on Electrical Resistivity Methods". GE 336 Lecture 11 notes.

5. Anderson, N. (2017). Lectures from: MASW and GPR, Environmental Applications of Geophysics. Missouri Unviersity of Science and Technology. Rolla, Missouri, USA.Anderson, Neil, Torgashov, Evgeniy. (2017). "Baumgartner to Fenton WWTF Tunnel: Geophysical Survey". Unpublished report for Shannon and Wilson, Inc.

6. Bansah, K. J., Anderson, N. L. (2017). "Multichannel Analysis of Surface Waves: Estimating Depth to Bedrock and Acoustic Properties in Karst Terrain". American Rock Mechanics Association.51st U.S. Rock Mechanics/Geomechanics Symposium, 25-28 June, San Francisco, California, USA.ARMA-2017-0082

7. Billington, N., Strohmeyer, J., & Rutledge, A. (2007). *2-D MASW Surveys to Evaluate Subsurface Stiffness: Investigations of the 2004 I-40 Landslide and Other Projects.* https://www.marshall.edu/cegas/geohazards/2007pdf/Session1/04%20Billington%20Geohazard%202007%20NEW.pdf

8. Coskun, N. "The effectiveness of electrical resistivity imaging in sinkhole investigations," International Journal of Physical Sciences, 7(15), 2398 - 2405. doi:10.5897/IJPS11.1063, 2012.Geologic Map of Missouri - PUB2514. (2014). In *Missouri Department of Natural Resources*. Retrieved March 22, 2020, from https://dnr.mo.gov/pubs/pub2514.pdf

9. Harrison, R. W. (1997). BEDROCK GEOLOGIC MAP OF THE ST. LOUIS 30' x 60' QUADRANGLE, MISSOURI AND ILLINOIS. Retrieved from USGS Publications Warehouse.

10. Hauck, H. S., & Harris, T. H. (n.d.). Water Resources Data - Missouri, Water Year 2005. In *U.S. Geological Survey Water Data Report MO - 05 - 1*. Retrieved March 22, 2020, from Water - Data Reports (WDRMO05 - Volume 1).

11. Howe, W. B. (1961, September). The Stratagraphic Succession in Missouri. In *Missouri Department of Natural Resources*. Retrieved from https://dnr.mo.gov/geology/adm/publications/documents/v-040-stratigraphic-succession.pdf

12. Jamaluddin, & Umar, Emi. (2018) Identification of Subsurface Layer with Wenner-Schlumberger arrays configuration geoelectrical method. IOP Conference Series: Earth and Environmental Science. 118. 012006. 101088/1755-1315/118/1/012006.

13. Kansas Geological Survey "Multichannel Analysis of Surface Waves", 2013 http:/www.masw.com/index.html

14. Kearey, Philip, Brooks, Micheal, Hill, Ian(1991) "An Introduction to Geophysical Exploration".

15. Loke, M.H.(1996-2016)"Tutorial : 2-D and 3-D Electrical Imaging Surveys".

16. Loke, M.H. (1999)"Electrical Imaging Surveys for Environmental and Engineering Studies".

17. Lowrie, William G.. (1997). "Fundamentals of Geophysics."

18. Miller, D. B., Emmett, L. F., Skelton, J., Jeffrey, H. G., & Barks, J. H. (1974). *Water Resources of the St. Louis Area, Missouri*. N.p.: Missouri Department of Natural Resources. Retrieved from https://dnr.mo.gov/geology/wrc/docs/WR30.pdf

19. Miller, R.D., Xia, J., Park, C.B., and Ivanov, J., 1999, "Multichannel Analysis of Surface Waves to Map Bedrock," *The Leading Edge*, 18(12), 1392-1396.

20. Miller, R. D., Xia, J., Park, C. B., & Ivanov, J. (1999). "Using MASW to Map Bedrock in Olathe, Kansas" In *Semanticscholar.org*. Retrieved from Semantic Scholar.

21. Missouri Department of Natural Resources. 1979. Geologic map of Missouri. Missouri Department of Natural Resources, Division of Geology and Land Survey, Rolla, Missouri.

22. Missouri Department of Natural Resources. 1984. Missouri water quality basin plans. Meramec, Whitewater and Castor River, Mississippi R., Joachim, Plattin, Establishment, Clinque Hommes and Apple creeks. Missouri Department of Natural Resources, Jefferson City, Missouri.

23. Missouri Department of Natural Resources. 1995a. Missouri water quality basin plans. Unpublished report of upper and lower Meramec River. Missouri Department of Natural Resources, Water Resource Division, Jefferson City, Missouri.

24. Mohamed, Adel & Ata, A.S.A. & Azim, F. & Taha, M.A.. (2013). Site-Specific Shear Wave Velocity Investigation for Geotechnical Engineering Applications Using Seismic Refraction and 2D Multi-Channel Analysis of Surface Waves. NRIAG Journal of Astronomy and Geophysics. 2. 88–101. 10.1016/j.nrjag.2013.06.012.

25. Muchaidze, I. (2008). Imaging in Karst Terrain Using Electrical Resistivity Tomography (Master's thesis). Retrieved from Scholar's Mine.

26. Nwokebuihe, S. C. (2014). *The Description of an Effective Sinkhole Investigation Approach: A Case Study of Two Sites in Greene County, Missouri* (Master's thesis). Retrieved from Missouri S&T Summon.

27. Obi, J. C. (2016). *Geophysical Imaging of Karst Features in Missouri* (Doctoral dissertation, ProQuest LLC, Ann Arbor). Retrieved from Missouri S&T Summon.Van Valkenburgh, Nooger and Neville (1992) "Basic Electricity".

28. Current, Resistance, and Resistivity review (2020). In *Khanacademy.org*. Retrieved from https://www.khanacademy.org/science/ap-physics-1/ap-circuits-topic/current-ap/a/resistance-and-resistivity-ap1

29. Identification of subsurface layer with Wenner-Schlumberger arrays configuration geoelectrical method - Scientific Figure on ResearchGate. Available from: https://www.researchgate.net/figure/Simplified-current-flow-lines-and-equipotential-surfaces-arising-from-a-a-single_fig1_323353321 [accessed 1 Apr, 2020]

30. Park, C.B. and Adkins-Heljeson, M.(2006) SurfSeis Active and Passive MASW User's Manual v 2.0. (Supplementary).Park, C.B., Miller, R.D. Xia, Jianghai, and Ivanov, Julian. (2007) "Multichannel Analysis of Surface Waves (MASW)-Active and Passive Methods". The Leading Edge

31. Choon B. Park, Richard D. Miller, and Jianghai Xia.(May-June 1999)."Multichannel Analysis of Surface Waves". GEOPHYSICS, VOL. 64, NO. 3.P. 800–808, 7 FIGS.

32. Park, C.B., Miller, R.D., & Miura, H. (2002). "Optimum Field Parameters of an MASW Survey".In *Semanticscholar.org*. Retrieved from Semantic Scholar.

33. Pires, J., Sotelo, D., Augustin, A., Osorio, V., De Paula, T., & Moura, C. (2019). *Application of Refraction Seismic on the Vulnerability of Underground Aquifers*.IOP Conference Series: Earth and Environmental Science. 221.012062.10.1088/1755-1315/221/1/012062 Retrieved from https://www.researchgate.net/figure/a-Extension-of-the-trigger-b-RAS-24-c-12v-battery-d-trigger-e-serial-cable-f-12_fig1_331452201

34. Resistivity Methods. (2016, May 18). Retrieved from https://archive.epa.gov/esd/archive-geophysics/web/html/resistivity_methods.html

35. Robinson, E.S. and Coruh, C., 1988. "Basic Exploration Geophysics."

36. Stokoe, K.H. & II, Wright & Bay, J.. (1994). Characterization of geotechnical sites by SASW method. https://www.researchgate.net/publication/238202052_Characterization_of_geotechnical_sites_by_SASW_method

37. Telford, W. M., Geldart, L. P., & Sheriff, R. E. (1990). *Applied Geophysics* (2nd ed.). Cambridge: Cambridge University Press.Tripathi, Ganesh. (2009). Use of Surface Geophysical Techniques to Locate a Karst Conduit in the Cane Run-Royal Spring Basin, Kentucky.http://www.mofossils.com/MOcolumn.html. Misssouri Stratigraphic column.

38. 2017 Statewide Geologic Map. (2017). Starbuck, Edith. A. Missouri Department of Natural Resources.

39. Springfield Plateau Ground water Province. Missouri Department of Natural Resources. https://dnr.mo.gov/geology/wrc/groundwater/education/provinces/springfieldplatprovince.html

40. https://dnr.mo.gov/geology/adm/publications/docs/map-SurfMap.pdf. Surficial Materials of Missouri. (2002). Missouri Department of Natural Resources.

41. Application of Refraction Seismic On the Vulnerability of Underground Aquifers - Scientific Figure on ResearchGate. Available from: https://www.researchgate.net/figure/a-Extension-of-the-trigger-b-RAS-24-c-12v-battery-d-trigger-e-serial-cable-f-12_fig1_331452201 [accessed 13 Apr, 2020]

42. Site-specific shear wave velocity investigation for geotechnical engineering applications using seismic refraction and 2D multi-channel analysis of surface waves - Scientific Figure on ResearchGate. Available from: https://www.researchgate.net/figure/The-Multi-channel-analysis-of-surface-waves-MASW-data-acquisition-configuration-for_fig16_259169858 [accessed 13 Apr, 2020]

VITA

Justin James Clinton grew up in Rolla, Missouri and has received a B.S. in Geology and Geophysics in May 2016. He received his master's degree in Geological Engineering from Missouri University of Science and Technology in December 2020. He had many opportunities to assist in different geophysical projects and reports while at Missouri S&T. In 2018, Justin Clinton began work with the USGS as an intern and began working full-time upon receiving his master's degree.